Pharmaceutical Research (2026) 43:465–482
https://doi.org/10.1007/s11095-025-04012-0

ORIGINAL RESEARCH ARTICLE

Enabling Anti-inflammatory Activity through Hyaluronan-coated PLGA Nanoparticles Loaded with Carvacrol

Saniya Salathia[1] · Dimitrios Agas[2] · Maria Rosa Gigliobianco[3] · Luca Boldrini[1] · Alessia Cappelli[2] · Cristina Casadidio[1] · Piera Di Martino[3] · Maria Giovanna Sabbieti[2] · Roberta Censi[1]

Received: 12 September 2025 / Accepted: 21 December 2025 / Published online: 13 January 2026

Abstract

Objective Chronic inflammation is characterized by excessive cytokine production and macrophage infiltration, contributing to disease progression. This study aimed to enhance the therapeutic efficacy and local delivery of carvacrol (CVL), a natural PPAR-γ activator with anti-inflammatory properties, through the development of a poly(lactic-co-glycolic) acid (PLGA)-based nanoparticle delivery system with hyaluronic acid (HA)-dependent macrophage targeting.

Methods Poly(lactic-co-glycolic) acid (PLGA)-based nanoparticles encapsulating CVL (CP NPs) were prepared and coated with 1.5% w/v hyaluronic acid (HA) to form CHP NPs for CD44 receptor-mediated targeting of pro-inflammatory macrophages. Physicochemical characterization, encapsulation efficiency, and drug release profile were evaluated. Cellular uptake and cytokine modulation were assessed in lipopolysaccharide-stimulated macrophages.

Results CP NPs exhibited a size of 155 ± 3 nm and a zeta potential of -57.7 ± 1.3 mV, while HA coating yielded CHP NPs with a size of 225 ± 18 nm and a zeta potential of -25.5 ± 0.3 mV. Encapsulation efficiency and loading capacity reached 91 ± 5% and 26 ± 7%, respectively. HA coating enhanced nanoparticle internalization by 41% compared to uncoated NPs. A sustained release profile was achieved, with 50 ± 13% of CVL released over 21 days. In macrophages, CHP NPs increased anti-inflammatory cytokines IL-1ra (+258%), IL-4 (+260%), and IL-10 (+40%), while reducing pro-inflammatory cytokines IL-1α (-25%), IL-1β (-36%), and TNF-α (-36%) relative to untreated cells.

Conclusions HA-coated PLGA nanoparticles effectively delivered CVL, enhancing macrophage targeting and promoting an anti-inflammatory response. This platform offers a promising strategy for treating chronic inflammation-related diseases.

Saniya Salathia and Dimitrios Agas contributed equally as first authors.

Maria Giovanna Sabbieti and Roberta Censi contributed equally as senior authors.

✉ Cristina Casadidio
cristina.casadidio@unicam.it

[1] School of Pharmacy, University of Camerino, ChIP Chemistry Interdisciplinary Project Research Centre, Via Madonna Delle Carceri, 62032 Camerino, MC, Italy

[2] School of Biosciences and Veterinary Medicine, University of Camerino, Via Gentile III da Varano, 62032 Camerino, MC, Italy

[3] Department of Pharmacy, "G. D'Annunzio" Chieti E Pescara Univeristy, Via Dei Vestini 1, 66100 Chieti, CH, Italy

Graphical Abstract

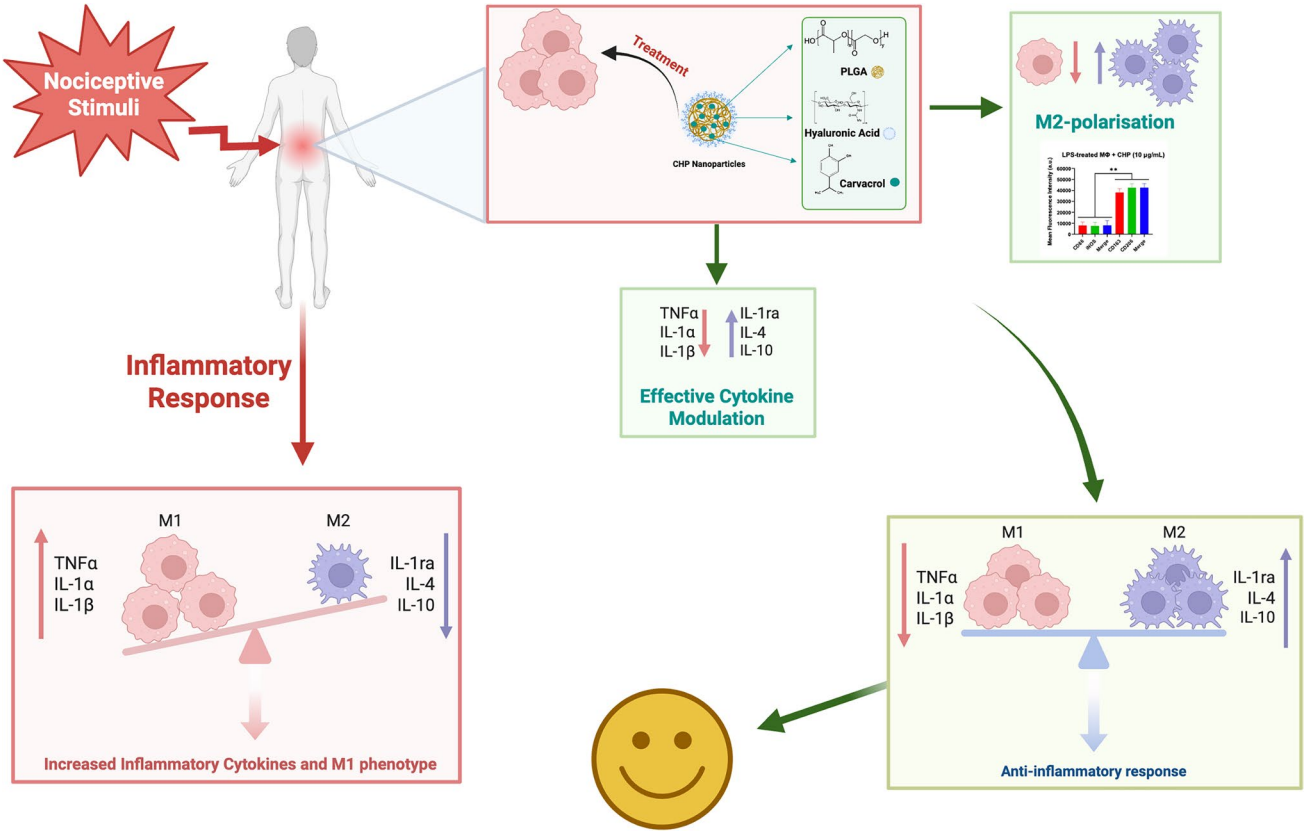

Keywords chronic inflammation · drug delivery · hyaluronic acid · macrophages · polymers

Introduction

Under adverse conditions, inflammation serves as the body first line of defense and as innate immune response, primarily regulated by macrophages [1, 2]. These macrophages exhibit remarkable plasticity, which determines the intensity and progression of inflammation through cytokine release. Macrophage plasticity encompasses a spectrum of phenotypes rather than a strict dichotomy between pro- and anti-inflammatory states. While macrophages are often categorized into pro-inflammatory (M1-m) and anti-inflammatory (M2-m) phenotypes, this classification represents only two extremes within a highly dynamic and context-dependent continuum [3–5]. In response to various microenvironmental cues, macrophages can adopt intermediate or hybrid states that exhibit overlapping functional properties [5]. Acute inflammation, typically driven by macrophages with an M1-like phenotype, plays a crucial role in maintaining homeostasis and protecting tissues from infection or injury [6]. However, the resolution of inflammation is a tightly regulated process involving multiple macrophage subsets with anti-inflammatory and tissue-repair functions. A failure to properly transition through these phenotypic states, particularly an inadequate shift toward pro-resolving macrophages, can result in chronic inflammation, leading to persistent tissue damage and contributing to diseases such as chronic pain [7].

Carvacrol (2-methyl-5-(1-methylethyl) phenol, CVL) is a phenolic monoterpene and a major constituent of oregano (*Origanum vulgare* L. with 66% abundance) and thyme (*Thymus vulgaris*) [8, 9], and it is widely recognized for its antibacterial [10], antimicrobial [11] and anti-inflammatory properties [12]. Furthermore, although CVL has a relatively high boiling point (~237 °C), its measured vapor pressure (2.96×10^{-2} mm Hg) suggests a certain extent of volatility, allowing evaporation under ambient conditions [13–15]. CVL anti-inflammatory action is mediated through the activation of peroxisome proliferator-activated receptor-γ (PPARγ), leading to the suppression of inflammatory cytokines like cyclooxygenase-2 (COX-2) production [16, 17], and interleukin-6 (IL-6), as proved in literature [18–20]. Despite its therapeutic potential, direct administration of free CVL may cause cytotoxicity in healthy cells, limiting its clinical applicability [21–23]. Yammine *et al.*

reported reduced toxicity of encapsulated CVL as compared to its free counterpart [24]. Therefore, encapsulation of CVL within nanoparticles has emerged as a promising strategy to mitigate this cytotoxicity by improving its biocompatibility and therefore effectively harnessing the anti-inflammatory mechanism of action [25].

One therapeutic strategy to resolve chronic inflammation involves the polarization of pro-inflammatory M1-m to anti-inflammatory M2-m phenotype [26]. To achieve this, such therapeutic nanosystem must specifically target M1 macrophages (M1-m) to ensure high efficacy. Hyaluronic acid (HA), a naturally occurring ligand, binds directly to the cluster of differentiation 44 (CD44) receptor, which is abundantly expressed on the surface of M1-m. This interaction facilitates receptor-mediated uptake of the nanosystem by M1-m [27]. Furthermore, the HA is extensively utilized in scientific research due to its versatility, with application in nanoparticles [28] and nanocarriers [29] development, often in combination with polymers [30], for the targeted delivery of therapeutic agents. To mention, the role of HA in the modulation of inflammation is widely acknowledged, however, it remains a subject of scientific debate. Indeed, while some studies suggest that low molecular weight (LMW) HA promotes inflammatory responses and high molecular weight (HMW) HA exhibits anti-inflammatory effects, other research presents conflicting evidence, challenging this dichotomy [31]. Nevertheless, HA remains a hot topic in nano drug delivery methods for cancer [29, 32, 33] and inflammatory diseases [34–36].

HA, being a weak acid, is characterized by its negative charge which allows it to be efficiently coated onto polymeric nanoparticles such as poly(lactic-co-glycolic acid) (PLGA) with the assistance of charged surfactants like cetyltrimethylammonium bromide (CTAB). This coating enhances the delivery of poorly water-soluble drugs by improving stability, bioavailability, and target specificity [37]. Polymeric nanoparticles offer a promising strategy to reduce the cytotoxicity but also overcome the volatility associated with the delivery of free drugs, allowing for their administration through various routes and enhancing their therapeutic potential [38, 39]. " Generally, carvacrol exhibits good chemical stability *in vitro*, however, following administration, its *in vivo* pharmacokinetic profile is largely governed by extensive biotransformation [40]. After entering circulation, carvacrol undergoes extensive oxidation and conjugation reactions, resulting in fast clearance from the bloodstream and contributing to adverse physiological effects such as hypotension and hypothermia [41–43]. These are metabolic and pharmacokinetic limitations rather than issues of intrinsic chemical instability. Encapsulation of CVL in PLGA nanoparticles helps overcome these challenges by reducing premature drug leakage and enabling a controlled and sustained release profile [10].

In this study, we developed a novel PLGA nanoparticle system encapsulating CVL to investigate its ability to target inflammation while preserving a hydrophobic environment for CVL loading. Furthermore, the HA coating on PLGA nanoparticles was performed to enable precise targeting of inflamed tissue, and macrophage uptake was evaluated. The impact of this system on inflammatory response modulation was highlighted through macrophage polarization and cytokine suppression. Overall, this study represents the first exploration of this targeted nanotherapeutic platform, providing new insights into its potential for inflammation management by demonstrating, for the first time, the combined effect of HA-coated and CVL-loaded PLGA nanoparticles on macrophage uptake and inflammatory response modulation.

Materials and Methods

Materials

Poly(lactic-co-glycolic acid) (PLGA) with a molecular weight of 17 kDa and acid-terminated structure (PURASORB PDLG 5002 A) was obtained from Corbion (Amsterdam, the Netherlands). Carvacrol (CVL) with a purity greater than 98.0% was purchased from TCI EUROPE N.V. (Zwijndrecht, Belgium). Hyaluronic acid (23 kDa) was supplied by ContiPro (Dolní Dobrouč, Czech Republic). Cetyltrimethylammonium bromide (CTAB) and bovine serum albumin (BSA) were sourced from Sigma-Aldrich (St. Louis, Missouri, United States). Dichloromethane (DCM), stabilized with ethanol, was provided by Carlo Erba (Milan, Italy). Distilled (DI) water was obtained with the apparatus RO 60 TS demi2 water deionizer provided by Gamma 3 Ecologia (Castelverde Costa Sant'abramo, Italy). The phosphate-buffered saline (PBS) used for the experiments was based on the 150 mM buffer solution at pH 7.4 of NaCl (136.9 mM), KH_2PO_4 (1.7 mM), and Na_2HPO_4 (13.4 mM).

For macrophage isolation, NCTC clone L-929 mouse fibroblasts cell line was obtained from ATCC (distributed by LGC, Milan, Italy) and cultured using Eagle Minimum Essential Medium (EMEM) (LGC, Milan, Italy). Additional reagents including fetal bovine serum (FBS), penicillin, streptomycin, and Roswell Park Memorial Institute (RPMI) 1640 Medium were purchased by Gibco, Life Technologies (Milan, Italy).

Hyaluronic Acid-coated PLGA Nanoparticles

The protocol for formulating PLGA nanoparticles was adapted and modified from Pradhan *et al.* [44]. Oil/water solvent evaporation method was used to develop PLGA

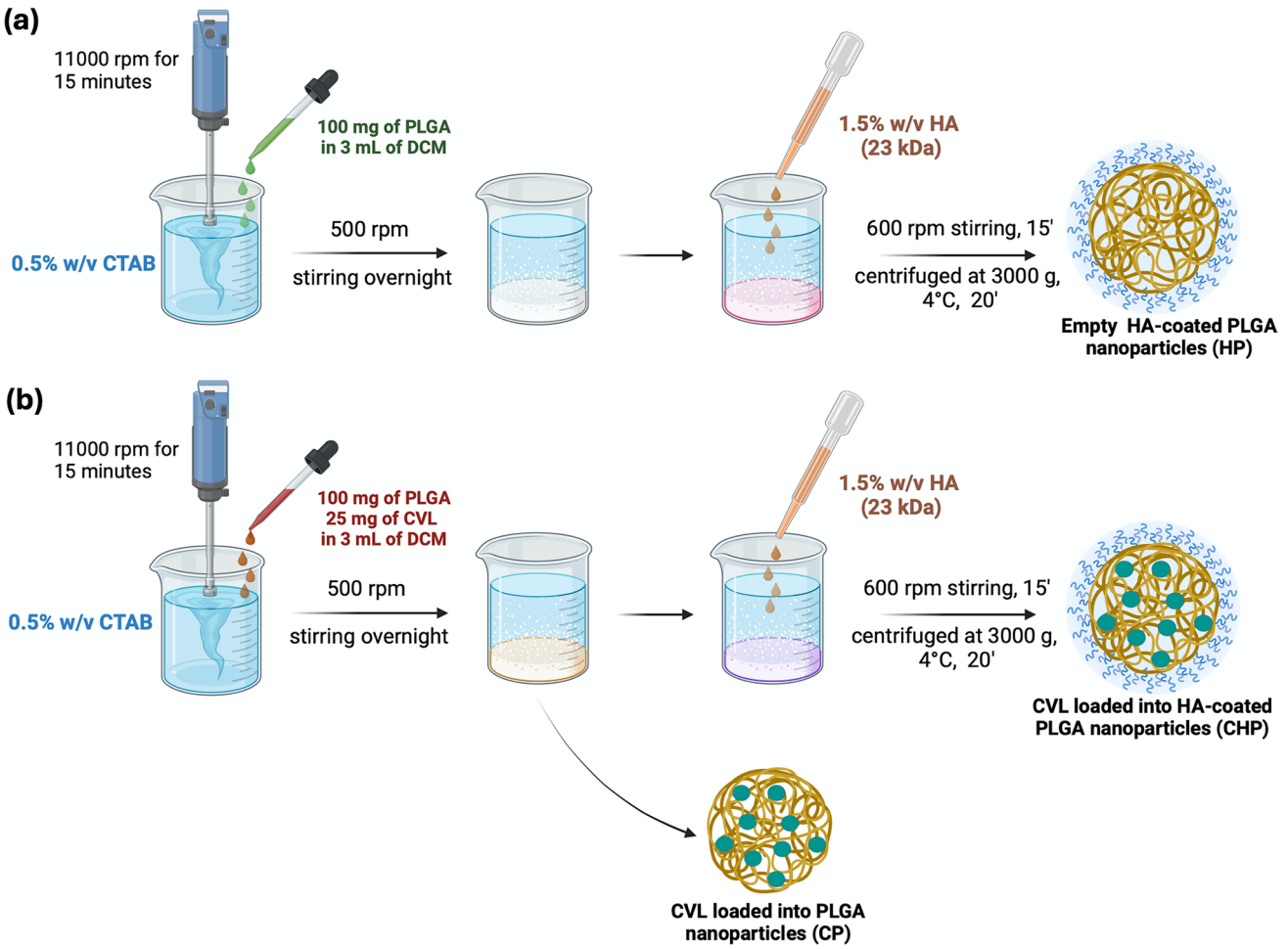

Scheme 1 Schematic representation of (**a**) HA-coated PLGA empty nanoparticles (HP NPs), and (**b**) CVL-loaded uncoated PLGA nanoparticles (CP NPs) and CVL-loaded HA-coated PLGA nanoparticles (CHP NPs). Partially created with BioRender.com.

nanoparticles where CTAB was used as a surfactant dissolved in the water phase (Scheme 1a). Briefly, a solution of 100 mg of PLGA dissolved in 3 mL of DCM was gradually added dropwise to an aqueous phase consisting of 18 mL of 0.5% w/v CTAB solution. To mention, CTAB is a quaternary ammonium surfactant with a positive charge, which enables it to ionically bind the surface of PLGA nanoparticles, thereby imparting a net positive surface charge to the nanoparticles [45, 46]. This positive charge facilitates the addition of HA, a negatively charged polysaccharide at physiological pH, by enabling electrostatic interactions with the cationic regions of the CTAB molecules. Afterwards, the emulsion was homogenized (T 25 digital ULTRA-TURRAX®) at 11,000 rpm for 15 min and left to stir at 500 rpm overnight in order to allow the solvent evaporation. To prepare HA-coated PLGA nanoparticles (Scheme 1a), 10 mL of a 1.5% w/v HA solution was added dropwise to the PLGA nanoparticles suspension. The resulting HA-coated PLGA nanoparticles were stirred for 15 min at 600 rpm and centrifuged at 3000 g and at 4˚ C for 20 min, favoring the removal of uncoated HA [44, 47]. The empty HA-coated PLGA nanoparticles (namely HP NPs) were then collected, freeze-dried and stored at −20°C until further use.

Carvacrol-loaded Nanoparticles

For the loading of CVL, 25 mg of CVL was dissolved in the organic phase mixture containing PLGA and DCM, and then added dropwise into the aqueous phase following the protocol described in Sect. "Hyaluronic Acid-coated PLGA Nanoparticles" (Scheme 1b). The resulting nanoparticles, CVL-loaded PLGA-nanoparticles (namely CP NPs) and CVL-loaded HA-coated PLGA-nanoparticles (namely CHP NPs) were freeze-dried and stored in the freezer (−20°C) until further use. The loading capacity and encapsulation efficiency was evaluated following the method described on Sect. "CVL Encapsulation Efficiency and Loading Capacity". All experiments were performed at least 4 times.

Nanoparticles Characterization

Size, PDI and Zeta Potential

The hydrodynamic diameter, polydispersity index (PDI) and zeta potential (ζ) of the formed nanoparticles were determined by Dynamic Light Scattering (DLS) technique with the Zetasizer Nano equipped with 633 nm HeNe (Malvern Instruments, Malvern, UK). For the measurements, 5 mg of freeze-dried HP, CP or CHP NPs, prepared following Sects. "Hyaluronic Acid- coated PLGA Nanoparticles" and "Carvacrol- loaded Nanoparticles", were suspended in 1 mL of DI water at 25 °C and an angle of 90°. All measurements were performed at 25° C and in triplicates. Data were corrected for viscosity using the Malvern Zetasizer software (version 8.01).

Scanning Electron Microscopy

The morphology of the CHP NPs (formulation described in Sect. "Carvacrol-loaded Nanoparticles") was evaluated by a field emission-scanning electron microscope ZEISS SIGMA 300 FESEM equipped with the Gemini column (1.2 nm @ 15 kV) (SEM, Zeiss Sigma 300, Zeiss, Germany). The dried CHP NPs sample was sputtered under vacuum with a chromium layer of approximately 100 Å thickness (Quorum Q150T ES, Quorum Technologies, Lewes, UK) before analysis. Conductive thin films (chromium and graphite) were deposited on the samples with the QUORUM Q150T.

Fourier-Transform Infrared Attenuated Total Reflectance (FT-IR ATR) spectroscopy

To highlight the presence of the HA coating on the PLGA nanoparticles, the chemical composition of the nanoparticles and the HA polymer was evaluated using FT-IR ATR analysis, performed with a PerkinElmer FT-IR spectrometer (Spectrum Two UATR) equipped with a ZnSe crystal (Waltham, Massachusetts, United States). The measurements were processed by a PerkinElmer data manager SpectrumTM 10 Software in a 400–4000 cm^{-1} range at a 2 cm^{-1} resolution and 4 scans.

CVL Encapsulation Efficiency and Loading Capacity

Gas Chromatography-Mass Spectrometry (GC–MS, Agilent GC–MS 8890 5790B, Milan, Italy) was used to calculate drug encapsulation efficiency (EE%) and loading capacity (LC%) following the Eqs. 1 and 2 respectively:

$$Encapsulation\ Efficiency\ (EE\%) = \frac{Amount\ of\ drug\ encapsulated}{Total\ drug\ added} \times 100 \quad (1)$$

$$Loading\ Capacity\ (LC\%) = \frac{Amount\ of\ drug\ encapsulated}{Total\ weight\ of\ nanoparticles} \times 100 \quad (2)$$

To prepare the samples for EE% and LC% analyses, 1 mL of acetone was added to 100 µL of the supernatant obtained from freshly prepared nanoparticles. The mixture was then centrifuged at 3000 × g for 10 min at 4 °C [48]. The supernatant was then collected and analyzed with GC–MS to estimate the non-encapsulated CVL. The instrument was equipped with an Agilent 7650 autosampler (Agilent, Santa Clara, California, USA). The samples were injected using an Agilent 5190–2295 Ultra Inert liner (Agilent, Santa Clara, California, USA). The injection volume was 1 µL, injector temperature was set at 250 °C and the injection was performed in split mode (10:1). The column was an Agilent HP-5MS (30 m*250 µm*0.25 µm) (Agilent, Santa Clara, California, USA). The gas used as carrier was Helium with a flow rate of 1.2 mL/min. The oven temperature was set at 40 °C held for 1 min, then it was increased with a rate of 20 °C/min up to 180 °C. Finally, the temperature was increased to 325 °C with a rate of 100 °C/min held for 4 min. Total runtime was 13.45 min. The molecules, after chromatographic separation, were ionized by electron ionization with the standard energy of 70 eV and analyzed by a single quadrupole. Ionization source and quadrupole were held, respectively, 230 °C and 150 °C. The MSD operated in SIM mode, monitoring the ions with a m/z of 91, 135, 150, with a dwell time of 100 ms each. The chromatograms were analyzed using the Agilent OpenLab CDS ChemStation Edition (Agilent, Santa Clara, California, United States).

For further verification, CP nanoparticles were mixed with 1 mL of acetone, centrifuged at 3000 g for 10 min at 4° C, and analyzed with GC–MS for measuring the amount of encapsulated CVL within the CP nanoparticles. It is important to note that CHP NPs with a hyaluronic acid (HA) coating were not tested due to the hydrophilicity of HA and its incompatibility with the GC–MS system. The tests were performed multiple times to ensure reliability and consistency of results (n = 4).

In vitro Drug Release Studies

The release studies were conducted on CHP NPs in phosphate-buffered saline (PBS, pH 7.4 composition given in Sect. "Materials") containing 4.5% w/v bovine serum albumin (BSA). Albumin-supplemented release media for drug release evaluation has been tested in literature to enhance solubility of hydrophobic drugs [49, 50]. Prior to release, the CVL solubility in 150 mM PBS + 4.5% w/v BSA was evaluated. For this, 1 mg of CVL was added to 4,6,8 and 10 mL of PBS + 4.5% w/v BSA solution and incubated at 37°

C overnight. Then, 500 µL of each sample was centrifuged at 10,000 rpm and 22° C for 20 min [48, 51]. Afterwards, 1 volume of supernatant (100 µL) was added to 10 × the amount of acetone and centrifuged at 5000 rpm for 10 min at 22° C. The samples were then tested with GC–MS. Based on the results, 8 mL of the media (PBS + 4.5% w/v BSA) per 1 mg of CVL was chosen for the release study.

To perform the release study, 3.85 mg of CHP NPs (corresponding to 1 mg of encapsulated CVL) was added to 28 mL of PBS + 4.5% w/v BSA solution and incubated at 37° C while continuously shaking (350 rpm) using an IKA vortex 4 digital (IKA®-Werke GmbH & Co. KG, Janke & Kunkel-Str. 10 79,219 Staufen, Germany). Sink conditions were maintained in the compartment during release studies. Aliquots were collected at different time points and prepared for GC–MS analysis as previously described [52, 53].

In vitro Anti-inflammatory Activity

Bone Marrow Macrophages Derivation

Collection of Feeder Layer from L-929 Fibroblasts NCTC clone 929 (L-929 cells) (ATCC; LGC Standards, Milano, Italy) were cultured in Eagle Minimum Essential Medium (EMEM) (ATCC; LGC Standards, Milano, Italy), 10% heat-inactivated-fetal bovine serum (HI-FBS; ATCC; LGC Standards, Milano, Italy), penicillin and streptomycin in the incubator at standard conditions (37 °C, 5% CO_2). Each 3 days, the medium was collected and filtered.

Bone Marrow Macrophages Isolation and Cultures Cell studies were performed using bone marrow derived macrophages (BMDMs) collected from 3-month-old C57BL/6 J male mice (Envigo, San Pietro Al Natisone, Italy). The mice used for bone marrow cell extraction partake to the Authorization number: 1044/2024-PR. Animals were sacrificed by carbon dioxide euthanasia and cervical dislocation. Femurs and tibia were removed, and the bone marrow was flushed by injecting Roswell Park Memorial Institute (RPMI) 1460 medium (Life Technologies, Milano Italy) into the bone cavity[54]. For macrophages isolation bone marrow cells (BMCs) suspension was plated in 100 mm dishes in presence of RPMI 1460 medium, supplemented with 10% HI-FBS, penicillin and streptomycin, 30% of the L-929 culture supernatant and the macrophage colony-stimulating factor (M-CSF) (Life Technologies, Milano, Italy) at the concentration of 10 ng/mL. The purpose of adding M-CSF is to stimulate monocytes to differentiate into neutral macrophages (M0), as previously demonstrated [55]. Cells were cultured until confluent, and the medium was replaced every 3 days thereafter.

Bone Marrow Macrophages Studies

Macrophages were detached using 0.25% trypsin–EDTA (Gibco, Life Technologies, Milano, Italy) and plated on coverslips (previously sterilized and inserted in six well culture plates) at the density of 10×10^4 cells/well. Cells were cultured in the supplemented medium. When macrophages reached 80% of confluence, some cultures were treated for 24 h with lipopolysaccharide (LPS; 150 ng/ml (Escherichia coli, Sigma-Aldrich) to polarize them toward the M1 inflammatory phenotype [56, 57] while the other were maintained in the only enriched medium. Subsequently, nanoparticles were added to the inflamed M1 and uninflamed M0 macrophages [56, 57]. Specifically, M0 and M1 macrophages were incubated with 1 mL of HP and CHP NPs at two different concentrations (5 µg/mL and 10 µg/mL). To explain, only CHP NPs contained CVL, with 1.3 µg and 2.6 µg of CVL, respectively. Additionally, 1 mL of free CVL with two different concentrations (2.6 µg/mL and 10 µg/mL) were tested to assess polarization and cytokine release. All the nanoparticle compositions are described in Sects. "Hyaluronic Acid- coated PLGA Nanoparticles" and "Carvacrol- loaded Nanoparticles".

Analyzing Macrophage Polarization

After 4 days of incubation with the nanoparticles and free CVL (see Sect. 2.6.2), cells were washed with PBS, (pH 7.4), fixed in 4% paraformaldehyde (PFA) and permeabilized with 0.3%v/v Triton X-100 for 20 min as previously described [58]. A method to study the M1 and M2 macrophages phenotype can be based on the evaluation of the expression of their specific markers through immunofluorescence analysis [59]. Thus, cultures were incubated for 2 h at room temperature with the following primary antibodies: a rabbit anti-CD86 (diluted 1:100) and a mouse anti-iNOS (diluted 1:50) (Life Technologies, Milano, Italy) to evaluate the expression of M1 markers; a mouse anti-CD206 Coralite 488 (diluted 1:50) and a rabbit anti-CD163 (diluted 1:50) (Life Technologies, Milano, Italy) to study the expression of M2 markers. After 3 washing with PBS (150 mM, pH 7.4), cells were incubated with the secondary antibodies Alexa fluor 488 chicken anti-mouse and Alexa fluor 594 goat anti-rabbit, both diluted 1:80, for 2 h. Cells were then washed 2 times with PBS and incubated for 45 min with DAPI (4′,6-diamidine-2′-phenylindole dihydrochloride; diluted 1:1000) at 37 °C. Finally, all cultures were washed 3 times with PBS and coverslips were mounted on slides in PBS/Glycerol 1:1. The slides were analyzed with a C2 Plus confocal laser scanning microscope (CLSM, Nikon Instruments, Florence, Italy). The microscope images were processed using NIS-Elements imaging software (Nikon Instrument, Florence, Italy). Controls were performed by samples incubation with the only secondary antibodies, or by complexing the primary antibodies

with the specific blocking peptide. The mean fluorescence intensity (MFI) was analyzed by a fluorometer Tecan Infinite (Tecan Infinite reader; Tecan, Milano, Italy).

Nanoparticle Internalization

Coating the nanoparticles with HA is motivated by its reported capability to bind to the CD44 receptor on M1 macrophages, facilitating enhanced cellular internalization [27, 60]. To observe the efficacy of HA-coated nanoparticles (CHP NPs) to internalize in M1-m, as compared to uncoated CP NPs, nanoparticle uptake was visualized by staining CHP and CP NPs with Nile red [61]. A Nile red stock solution of 1 mg/mL was prepared, out of which 10 µL was added to the PLGA organic phase. The nanoparticles were further prepared like stated in Sects. "Hyaluronic Acid- coated PLGA Nanoparticles" and "Carvacrol- loaded Nanoparticles". For the cell analyses, LPS-treated BMDMs were incubated with 1 mL of working nanoparticle (CP and CHP NPs) concentration of 10 µg/mL for 24 h. The uptake was studied by quantifying the fluorescence signal of Nile red. Specifically, the mean fluorescence intensity (MFI) was measured by a fluorometer Tecan Infinite (Tecan Infinite reader; Tecan, Milano, Italy).

Evaluating Cytokine Production

To further verify the anti-inflammatory effect of CVL, the expressions of certain inflammatory cytokines was also analyzed. The cells were treated as in Sect. Bone marrow macrophages studies, and the supernatant was collected after 48 h. The amount of different pro- (IL-1α/1β and TNF- α) and anti- (IL-1ra/4/10) inflammatory cytokines was tested with Mouse Cytokine Array Panel A kit (R&D Systems). Immunoreactive spots were quantitated densitometrically using ImageJ software.

Statistical Analysis

The p values were determined by a Student's test with two-tailed distribution performed with the software GraphPad Prism 9 (GraphPad Software Inc., La Jolla, California), where p values < 0.05 are considered statistically significant ($^{*}p < 0.05$, $^{**}p < 0.01$).

Results and Discussion

Nanoparticles Characterization

The hydrodynamic diameter of the formulated nanoparticles was characterized using dynamic light scattering (DLS), as summarized in Fig. 1a. The size of the empty PLGA nanoparticles was determined to be 162 ± 2 nm with a low polydispersity index (PDI) of 0.09 ± 0.03, indicating a narrow size distribution. Consistent with previous studies [44, 47], the incorporation of hyaluronic acid (HA) led to a significant increase in HA-coated PLGA nanoparticles (HP NPs) size, reaching 285 ± 17 nm (PDI 0.39 ± 0.01). This trend aligns with findings by Pradhan *et al.* [44], who reported a size increase proportional to the concentration of HA. Additional details on the effects of varying HA concentrations and molecular weights on nanoparticle size optimization are provided in the supplementary materials accompanying this paper (Table S1 and Figure S1, Supporting Information). Encapsulation of carvacrol (CVL) into PLGA resulted in CP nanoparticles with a mean hydrodynamic size of 155 ± 3 nm and a low PDI of 0.07 ± 0.03, indicating a uniform size distribution. Also in this case, HA-coated CP nanoparticles (CHP NPs) increased the size to 225 ± 18 nm with a higher PDI of 0.34 ± 0.12, reflecting a broader size distribution. Morphological analysis using scanning electron microscopy (SEM) revealed an overall smaller CHP nanoparticle distribution size than the one determined by DLS (Fig. 1b). This discrepancy is likely due to differences in measurement conditions between the two techniques. Specifically, the larger size observed in DLS measurements can be attributed to sample preparation, where nanoparticles are suspended in water. This suspension can lead to water absorption by the highly hydrophilic hyaluronan coating and subsequent swelling of the nanoparticles. The swelling effect is particularly pronounced due to the hygroscopic nature of HA, whose negatively charged subunits promote water retention [62]. This phenomenon highlights the influence of surface modification on nanoparticle behavior in aqueous environments and suggests that the hydrodynamic size measured by DLS may more closely reflect the functional state of nanoparticles in biological conditions [63]. In contrast, SEM analysis requires dried samples, which eliminates the possibility of nanoparticle swelling due to water absorption. Consequently, the smaller size of the nanoparticles observed in SEM images reflects their dehydrated state, minimizing the influence of HA-induced water retention.

The surface charge (ζ-potential) of empty PLGA nanoparticles was measured at $+57.7 \pm 1.3$ mV, attributed to the addition of CTAB as a surfactant. However, upon coating with HA to form CHP NPs, the ζ-potential of HP NPs decreased significantly to -25.5 ± 0.3 mV. This shift in charge can be attributed to the anionic nature of HA, stemming from its carboxyl groups, which aligns with the expected negative surface charge conferred by HA. These findings underscore the significant impact of HA coating on both particle size and surface charge, which are critical parameters influencing nanoparticle stability and interaction with biological systems.

(a)

Sample	Size (nm)	PDI	ζ-potential (mV)
PLGA	162±2	0.09±0.03	57.7±1.3
HP	285±17	0.39±0.01	-25.5±0.3
CP	155±3	0.07±0.03	16.7±1.1
CHP	225±18	0.34±0.12	-26.7±2.2

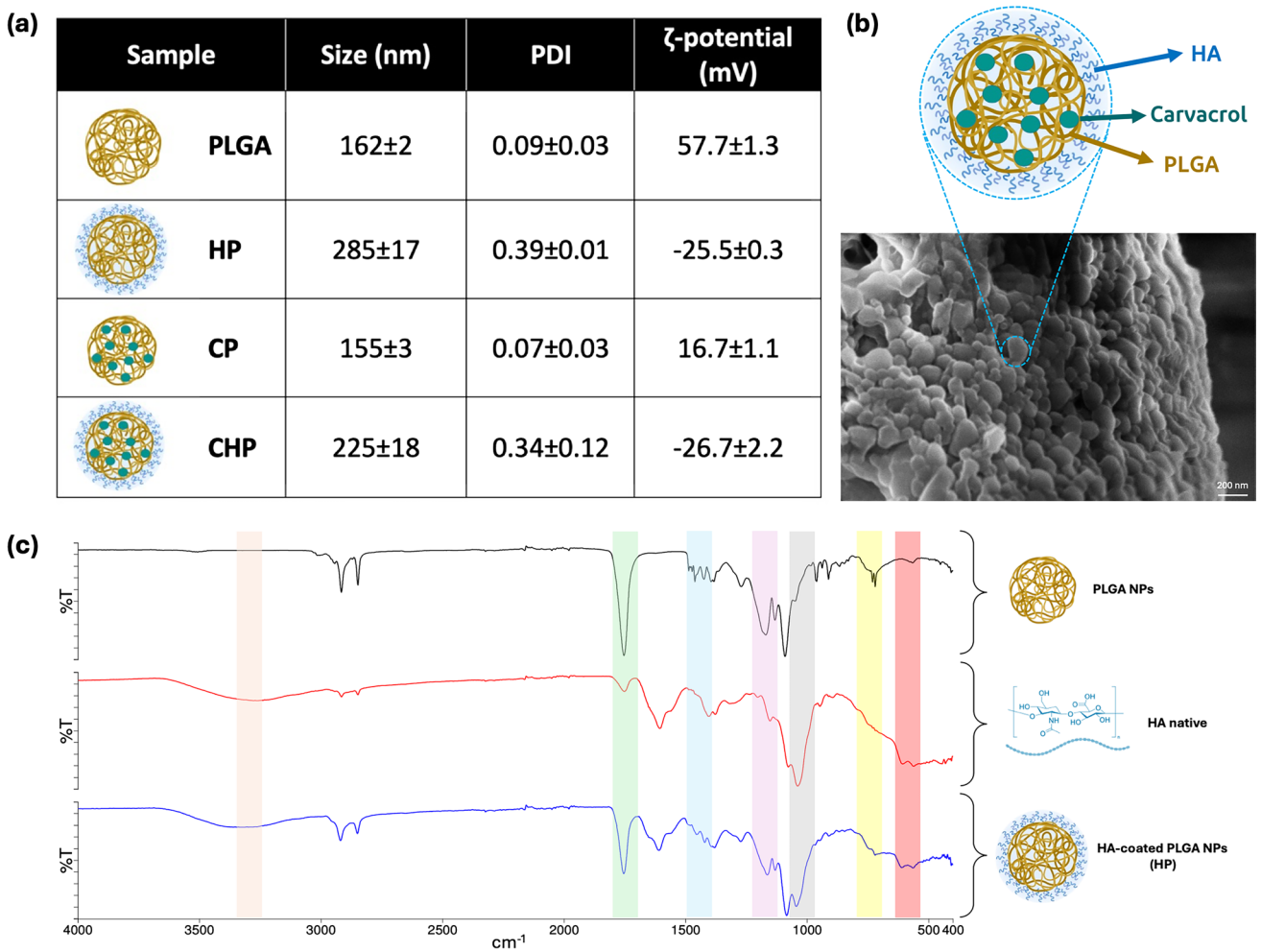

Fig. 1 (**a**) Size, PDI, and zeta potential (ζ) of all the prepared nanoparticles (n = 3, mean ± SD); (**b**) SEM analysis of CHP NPs, highlighting the smaller nanoparticle size observed compared to DLS measurements; (**c**) FT-IR spectra of PLGA nanoparticles (black), native hyaluronic acid (HA) (red), and HA-coated PLGA nanoparticles (HP NPs) (blue), confirming the successful coating of PLGA with HA through characteristic peaks. Partially created with BioRender.com.

CVL is known for its high encapsulation efficiency profile in polymers [64, 65]. Using Eq. 1, the encapsulated CVL accounted for 90.8 ± 5.2%, with a loading capacity (LC%) of 26.0 ± 6.6%, as calculated using Eq. 2. These results demonstrate the effectiveness of the single-emulsion solvent evaporation method used in this study. Furthermore, even after lyophilization, carvacrol remains within the nanoparticles, indicating the effective encapsulation of the molecule.

In comparison, a previous study reported a CVL encapsulation efficiency of ~ 26% in PLGA nanoparticles prepared using the solvent displacement method [10]. In contrast, our method demonstrated a substantial improvement, tripling the encapsulation efficiency (~ 90%). Additionally, the LC% increased from the reported ~ 21% to ~ 26% in our formulation, which correlates with the significant improvement in EE%. This improvement highlights the advantages of the single-emulsion solvent evaporation method, which appears to provide a more favorable environment for the efficient encapsulation of CVL.

Furthermore, the FT-IR spectra confirmed the successful coating of PLGA nanoparticles with hyaluronic acid (HA) by displaying characteristic peaks from both components (Fig. 1c). The spectrum of PLGA nanoparticles (black) shows distinct absorption bands, including a strong C = O stretching vibration at ~ 1750 cm^{-1}, characteristic of ester bonds, C-O stretching in the range of 1180–1080 cm^{-1}, and C-H stretching near 2990–2940 cm^{-1}. Native HA (red) exhibits key peaks such as a broad O–H stretching vibration between 3300–3400 cm^{-1}, indicative of hydroxyl groups, as well as amide I (1650 cm^{-1}) and amide II (1550 cm^{-1}) bands, which correspond to the amide bonds in HA. Additionally, C–O–C stretching vibrations around 1070–1030 cm^{-1} confirm the polysaccharide structure of HA. The HA-coated PLGA nanoparticles (blue) spectrum retains the key features

of both PLGA and HA, demonstrating successful coating. The presence of the broad O–H stretching (3300–3400 cm^{-1}), amide I and II bands (~ 1650 cm^{-1} and ~ 1550 cm^{-1}), and C–O–C stretching near 1070–1030 cm^{-1} confirms the presence of HA, while the retained C = O stretching at ~ 1750 cm^{-1} indicates the integrity of the PLGA core. These findings align with literature values [30, 66, 67] and confirm the successful functionalization of PLGA nanoparticles with HA, which is essential for applications such as targeted drug delivery and biomaterial engineering.

In addition, the preservation of physicochemical properties over time is a critical aspect for therapeutic nanosystems to ensure formulation reproducibility. To minimize potential degradation and aggregation phenomena during storage, all nanoparticle formulations were lyophilized and stored at − 20 °C as a precautionary measure. This storage condition was selected to preserve nanoparticle integrity during the study period, rather than to define long-term shelf life.. To prevent aggregation and maintain nanoparticle stability during the freezing and drying processes, a cryoprotective agent is typically added. Common cryoprotectants include saccharides such as sucrose or trehalose. However, in this study HA, a polysaccharide already present in the drug delivery system, serves as an intrinsic cryoprotectant. HA helps reduce crystal growth and create a stabilizing, hydrated network around nanoparticles, limiting aggregation under lyophilization conditions [68–70]. After 4 months of storage, HP NPs exhibited a mean size of 201 ± 2 nm with a PDI of 0.17 ± 0.01, indicating a stable size distribution. However, by 6 months, the particle size increased significantly to 649 ± 43 nm with a PDI of 0.75 ± 0.20, suggesting the onset of aggregation or instability. In contrast, CHP NPs demonstrated less stability, indeed their size was already 661 ± 114 nm and 0.55 ± 0.19 of PDI after 2 months of storage at −20 °C. Under these storage conditions, empty HP NPs maintained their physicochemical stability, particularly in terms of particle size, for up to 4 months. In contrast, CVL-loaded CHP NPs showed a progressive reduction in stability. This behavior is likely attributable to the presence of the encapsulated drug, which may impose additional stress on the polymeric matrix and promote aggregation phenomena over time. [71]. Future optimization of the formulation or storage conditions may help mitigate this issue and enhance the shelf life of drug-loaded nanosystems.

Furthermore, to prove the advantages of the presented nanosystems, an evaporation study was conducted where 1 mg of free CVL and CHP (encapsulating 1 mg CVL) were placed in an open vial at room temperature, and their weight was measured at different time points. After 24 h, a ~ 13% drop was observed in the pure CVL weight, whereas only a ~ 5% weight drop was noticed in CHP after 3 days (Figure S2, Supporting Information). After 96 h, more than 50% of pure CVL was noted to be evaporated. As discussed earlier, the mass loss observed for CVL is attributed to its low vapor pressure, which enables gradual evaporation of the compound over time, ultimately resulting in the reduced weight measured at the end of the study. This study confirmed that the encapsulation of CVL in CHP can improve its shelf life and evaporation rate, which is essential for its use further studies.

Carvacrol Release Studies

The release profile of CVL from HA-coated PLGA nanoparticles was monitored over 66 days in PBS + 4.5% w/v BSA media under sink conditions (Fig. 2). BSA was included in the release medium to enhance the solubility of hydrophobic compounds, ensuring accurate measurement of its release kinetics [50, 51]. Equation 3 was applied to investigate the release kinetics of CVL from HA-coated PLGA nanoparticles and to characterize the underlying mechanisms governing its release profile. Using this approach, distinct phases in the release profile were identified. The burst release phase exhibited a 19 ± 1% CVL release, whereas ~ 30% of the drug underwent release over the next 21 days, reaching ~ 50% of CVL released. The first part of CVL release can be attributed to the amount of drug encapsulated close to the surface of PLGA nanoparticles or drug adsorbed to the external surface, which characterizes the burst release phenomenon. Specifically, 14 ± 1% of the drug was released immediately at the first time point (1 h), as the drug located on the surface becomes rapidly stripped away in an uncontrolled manner by the release medium. Between 14 and 19% release, the drug requires approximately 6 h to dissolve, exhibiting a nearly constant release rate that resembles a zero-order profile. This portion of the release is attributed to desorption processes, reflecting the disruption of weak interactions between the polymer matrix and CVL. Subsequently, a second phase with a similar zero-order–like trend is observed, likely governed by the gradual degradation of PLGA. In this final phase, drug release relies on the gradual degradation of the polymeric nanoparticles, ensuring a sustained and controlled delivery over 21 days. Indeed, PLGA is a well-known drug carrier for its biodegradability but notorious for its slow-release profile [72–75]. The review by Fredenberg *et al.* [75] described the various mechanisms of drug release from PLGA noting many studies that reported the adsorbance of BSA on PLGA and subsequent delayed drug release. Moreover, a strong drug-polymer interaction can also cause a slow release [76, 77]. Considering that the nanoparticles were coated with a highly hydrophilic HA, it is possible that the initial burst release noticed may have been due to the release of the CVL close to the surface of PLGA caused by diffusion through water absorbed by the HA. Once this

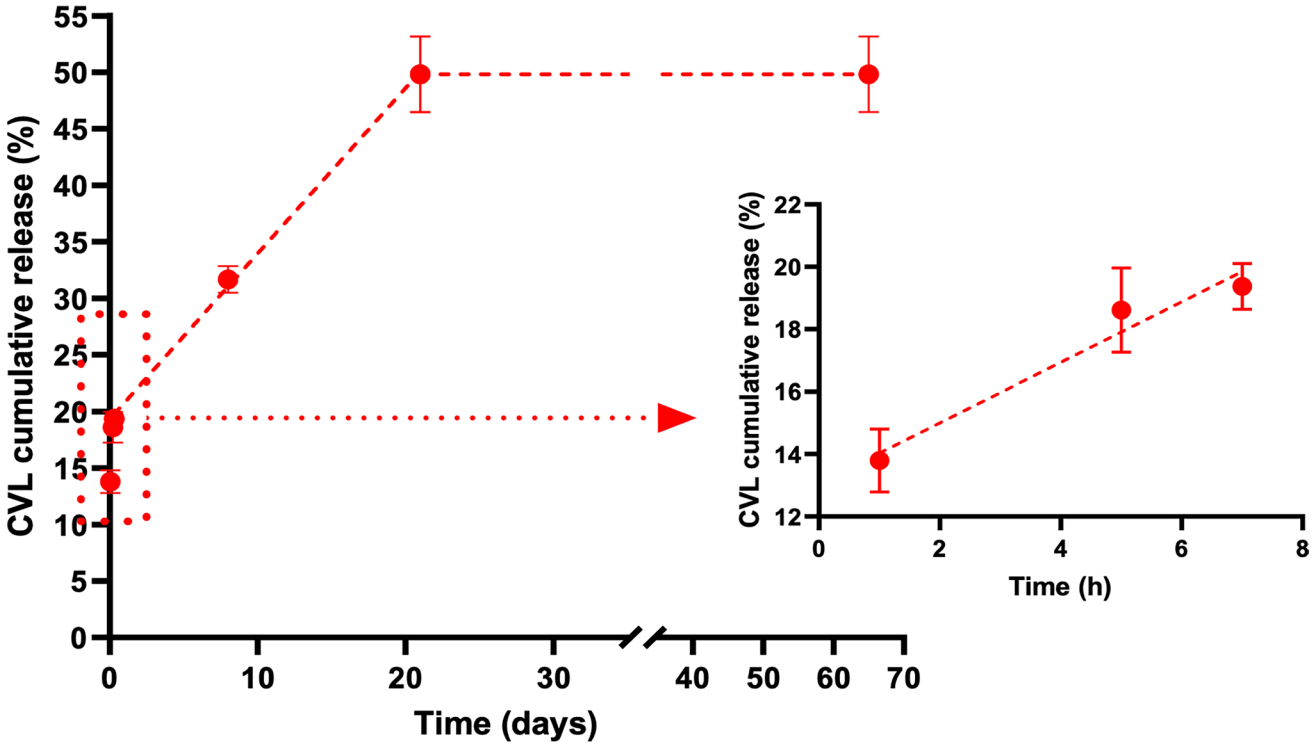

Fig. 2 The cumulative release profile of CVL from CHP NPs in PBS with 4.5% w/v BSA was analyzed using GC–MS. A burst release of CVL was observed in the first 7 h, followed by a sustained release until day 21. Data are presented as mean ± SD ($n = 3$).

initial phase is over, the subsequent drug release is attributed to the aliquot of the drug encapsulated deep within the core of the nanoparticles. This phase likely involves the erosion of the nanoparticle and/or the release of the drug from the polymer matrix through further water absorption. Both mechanisms are expected to occur slowly due to the inherently slow-degrading nature of PLGA.

Overall, a prolonged release of ~ 50% CVL in the first 21 days was observed. Notably, the release was monitored until day 66, with no further increase in the percentage of CVL released. A similar slow drug release profile of CVL from chitosan nanoparticles was also reported by Keawchaoon *et al.* [78]. The study reported triphasic release profiles in different pH media for over a span of two months. A more acidic buffer (pH 3) was observed with the highest release rate of 52%, while pH 7–11 reported release rates of 22–33%. In another study performed by Niza *et al.*, CVL encapsulated in polylactide showed an incomplete release at 37˚C (pH 7.4) [79]. This release profile was enhanced by modifying the pH to acidic conditions and/or performing the experiments at higher temperatures. This is in line with our studies where BSA was used in the release media which has a reported pH range of 4–9. While our study employed PLGA nanoparticles and HA, it can be said that CVL has an inherent nature of a slow-release profile. Other studies have also mentioned significant loss in the amount of CVL during the release studies which may amount to lower cumulative drug released [80]. Furthermore, release studies from Taghipour *et al.* reported aggregation of BSA around the PLGA nanoparticles, which leads to the formation of protein corona, significantly hampering the cumulative release of drugs from the core of the nanoparticles [81]. Even though the outer coating of HA can significantly reduce the adsorption of proteins, still remains a possibility of its formation [82, 83]. Therefore, the combined effects of CVL evaporation, non-acidic conditions, and potential protein corona formation result in incomplete CVL release from CHP NPs.

Nanoparticle Uptake by M1 Macrophages

A targeted drug delivery system is essential for maximizing therapeutic efficacy while minimizing unintended effects. By reducing damage to nearby healthy cells, such systems improve patient outcomes and reduce adverse effects [84, 85]. In this study, HA was utilized to enhance the precision of CVL-loaded PLGA nanoparticles delivery specifically to M1 macrophages (M1-m). This targeted approach is crucial, as it ensures that the therapeutic effects are concentrated solely on the intended cells. The difference in cellular uptake after 24 h of incubation of PLGA nanoparticles co-loaded with CVL and Nile red, with and without HA coating, is

depicted in Fig. 3. Before nanoparticles incubation, M1-m cells were pre-treated with lipopolysaccharide (LPS). LPS pretreatment is crucial for nanoparticle uptake studies involving M1 macrophages because it polarizes the macrophages toward a pro-inflammatory state, mimicking conditions seen in infection or disease [86]. M1 macrophages, characterized by their heightened phagocytic activity and cytokine production, provide a realistic and physiologically relevant model to evaluate how nanoparticles interact with activated immune cells [87]. This step ensures accurate assessment of nanoparticle efficacy, targeting potential, and safety under inflammatory conditions, which are often the therapeutic focus in drug delivery or immunomodulation research.

Notably, LPS-treated M1-m cells incubated with HA-coated CVL-loaded PLGA nanoparticles (CHP NPs) exhibited a significant increase in total mean fluorescence intensity (MFI) compared to uncoated CVL-loaded PLGA nanoparticles (CP NPs). Nile red, a hydrophobic fluorescent dye, was chosen to label the nanoparticles due to its strong affinity for lipid-rich environments and co-loaded with CVL. It shares the same hydrophobic nature as CVL, making it an ideal marker for tracking the distribution and uptake of CVL-loaded nanoparticles [88]. Specifically, the MFI recorded was 33,453 ± 3,599 a.u. for CHP NPs while a signal of 47,055 ± 4,544 a.u. was noted for CP NPs. This represented approximately a + 41% higher fluorescence signal when the nanoparticles were coated with HA, indicating enhanced uptake. The observed increase is attributed to HA functioning as a direct ligand for the CD44 receptor on the M1-m surface, facilitating receptor-mediated endocytosis and improving nanoparticle internalization. The observed increase in uptake due to HA coating aligns with previous studies [1, 51], further validating the role of HA in enhancing macrophage-specific targeting. These findings underscore the potential of HA-functionalized nanoparticles as a robust platform for targeted drug delivery, offering a compelling strategy to improve therapeutic outcomes.

Macrophage Polarization

Macrophages exhibit remarkable plasticity, enabling them to polarize into either a pro-inflammatory (M1) or an anti-inflammatory (M2) phenotype in response to environmental stimuli. This dynamic polarization plays a critical role in immune regulation and has significant implications for the development of targeted therapies for inflammatory diseases [89–91]. In this study, LPS treatment was employed to polarize macrophages into the M1 phenotype effectively, as evidenced by the significantly higher expression of M1 markers CD86 and iNOS compared to M2 markers CD163 and CD206. This polarization model provided a robust framework to evaluate the effects of CVL-loaded HA-coated PLGA nanoparticles (CHP NPs) on macrophage phenotype modulation.

The study revealed that treating M1-polarized macrophages with 5 µg/mL of CHP NPs (containing 1.3 µg of CVL) led to a modest increase in the M2 marker CD163 (+ 93%), indicating limited polarization resistance at this concentration (Fig. 4). However, when the CHP NPs concentration was increased to 10 µg/mL (containing 2.6 µg/mL of CVL), the effects became striking. Specifically, M1 markers CD86 and iNOS were drastically reduced (−83% and −84%, respectively), while M2 markers CD163 and CD206 were significantly elevated (+ 321% and + 399%, respectively). These results demonstrate a clear dose-dependent effect, reinforcing the potency of CHP NPs in shifting macrophages from a pro-inflammatory to an anti-inflammatory state. This

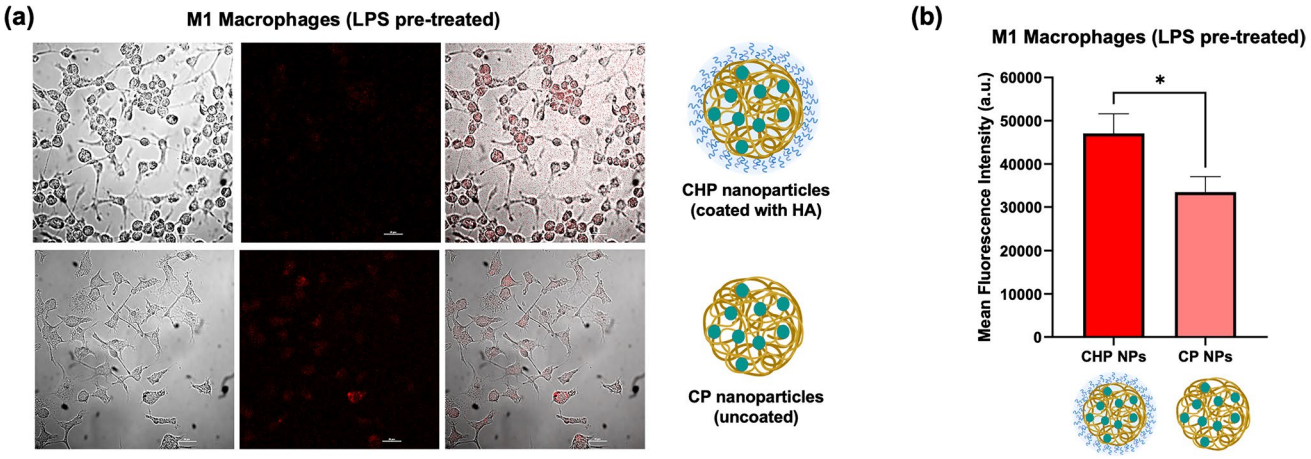

Fig. 3 Uptake of PLGA (CP) and HA-coated PLGA (CHP) nanoparticles (NPs) co-loaded with CVL and Nile red by M1 macrophages (M1-m). (**a**) Confocal laser scanning microscopy (CLSM) images of M1-m monocultures after 24 h of incubation with CP and CHP NPs at 37 °C, showing intracellular NPs localization. Partially created with BioRender.com. (**b**) Quantification of total mean fluorescence intensity (MFI) as described in Sect. 2.3.7, indicating the extent of NPs uptake. Data are presented as mean ± SD ($n = 6$), with $^*p < 0.05$. Scale bar = 20 µm.

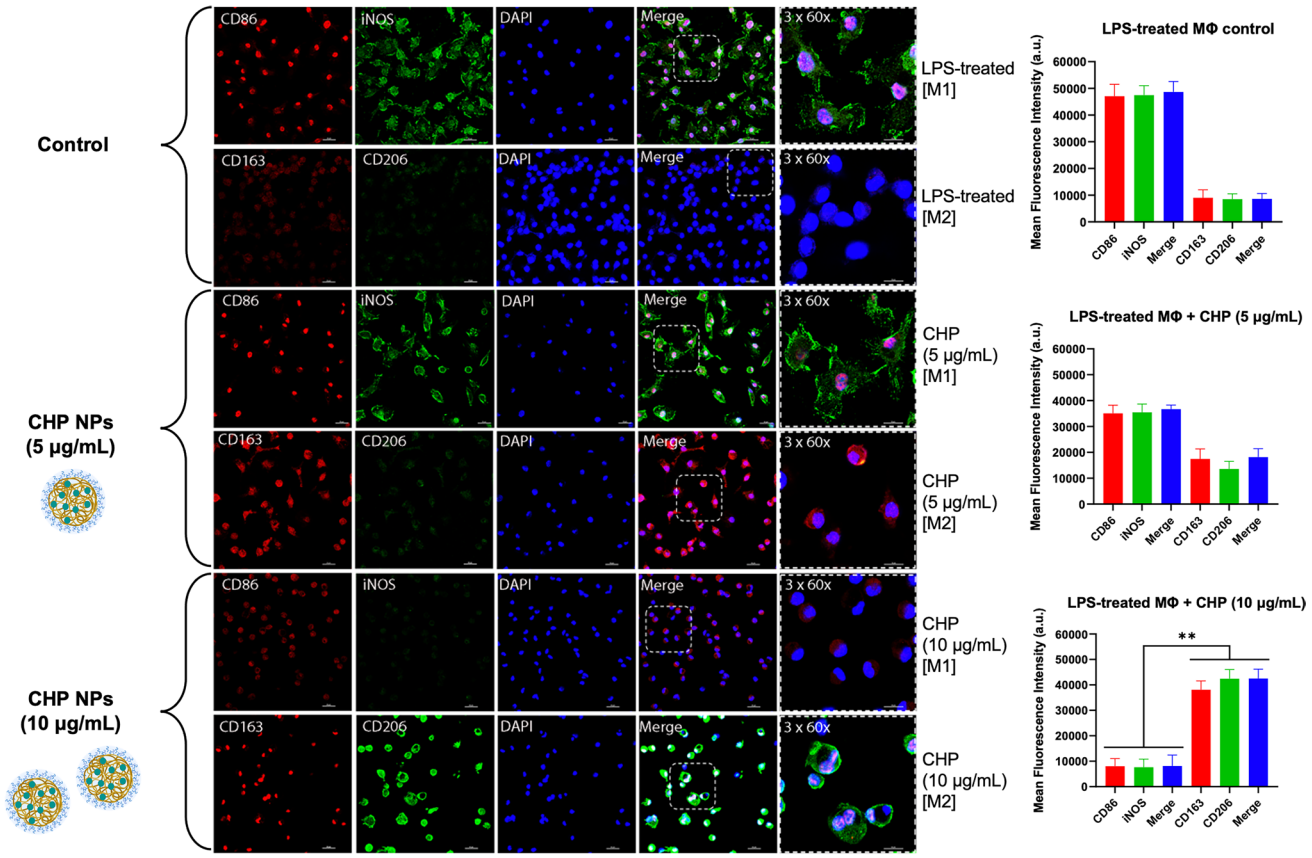

Fig. 4 LPS pre-treated macrophages were incubated with different concentrations of CHP NPs (CHP NPs). CHP NPs with 5 µg/mL concentration showed a lower polarization of M1 macrophages to M2 macrophages, as compared to a higher CHP NPs concentration of 10 µg/mL. The total MFI was calculated as described in Sect. 2.3.7. All values are expressed as mean ± SD (n = 6), with **p < 0.01.

underscores the importance of optimizing CHP NPs concentrations for effective therapeutic outcomes.

To further investigate the synergistic effects of CVL and HA-coated PLGA nanoparticles, parallel experiments were conducted using equivalent (2.6 µg/mL) and higher (10 µg/mL) concentrations of naked CVL and unloaded HA-PLGA nanoparticles (HP NPs). In all the control groups (Fig. 5), the formulations showed negligible effects on macrophage polarization, with minimal changes in M1 and M2 markers. At CVL 10 µg/mL, naked CVL-treated macrophages exhibited an ambiguous phenotype, with moderate reductions in CD86 (−40%) and iNOS (−38%) but only limited increases in CD163 (+ 115%) and CD206 (+ 189%), indicating a lack of strong polarization in either direction. Similarly, treatment with HP NPs at 10 µg/mL failed to elicit a significant M2 response. Overall, these findings highlight the critical role of HA-mediated targeting and sustained CVL release in maximizing therapeutic efficacy. Unlike naked CVL and placebo HP NPs, which displayed only partial or inconsistent effects, CHP NPs effectively suppressed pro-inflammatory M1 markers while robustly enhancing M2 polarization. This underscores the novel synergistic potential of CHP NPs in immune modulation, paving the way for its application in inflammation-related therapies. Therefore, the HA coating of the PLGA nanoparticles plays a pivotal role in targeting macrophages and enhancing therapeutic outcomes. HA affinity for CD44 receptors, which are overexpressed on activated macrophages, facilitates selective uptake of CHP NPs by the target cells [1, 27, 60]. This targeted delivery mechanism likely contributes to the enhanced anti-inflammatory effects observed with CHP NPs treatment. Additionally, the HA coating may improve nanoparticle stability and biodistribution, further augmenting their efficacy.

An important observation was the dose-dependent toxicity associated with higher concentrations of CVL and CHP NPs (Figs. 4– 5), necessitating the exclusion of higher doses from the study to maintain cell viability. While 10 µg/mL of CHP NPs was identified as an effective concentration for macrophage polarization, higher doses led to significant cytotoxicity, underscoring the delicate balance between therapeutic efficacy and safety in nanoparticle-based drug delivery systems (data not shown). This finding highlights the importance of optimizing nanoparticle formulations and dosing regimens to minimize off-target effects while maximizing therapeutic benefits.

Modulation of Inflammatory Cytokine Production

The production of inflammatory cytokines plays a pivotal role in regulating the inflammatory response at the site of injury or infection. These signaling molecules orchestrate the activation, resolution, or amplification of the immune response, and their balance is critical in determining the progression of inflammation [12, 34]. To better understand the therapeutic potential of the CHP NPs, the cytokines expression profile of LPS-treated macrophages was analyzed for both pro-inflammatory cytokines (IL-1α, IL-1β, TNF-α) and anti-inflammatory cytokines (IL-1ra, IL-4, IL-10). The detailed results are illustrated in Fig. 6. In LPS-stimulated macrophages, a hallmark of inflammation is the robust production of pro-inflammatory cytokines such as IL-1α, IL-1β, and TNF-α [34, 92, 93]. After treatment with 10 µg/mL of CHP NPs, a substantial reduction in these pro-inflammatory mediators was observed. Specifically, IL-1α expression decreased by −25%, IL-1β by −36%, and TNF-α by −36%, as shown in Fig. 6a-c. These reductions highlight the ability of CHP NPs to suppress key inflammatory pathways, likely due to the sustained release of CVL and HA-mediated targeted delivery. TNF-α, a pivotal cytokine that amplifies the inflammatory cascade, was notably reduced, indicating that CHP NPs could effectively disrupt the inflammation feedback loop. Similarly, IL-1α and IL-1β, which contribute to tissue damage and immune cell recruitment, were significantly downregulated, reinforcing the broad anti-inflammatory potential of CHP NPs treatment. In addition to reducing pro-inflammatory cytokines, CHP NPs treatment markedly increased the levels of anti-inflammatory cytokines. As depicted in Fig. 6d-f, IL-1ra expression increased by + 258%, IL-4 by + 260%, and IL-10 by + 40% following CHP NPs administration. These cytokines play essential roles in resolving inflammation and promoting tissue repair, further supporting the therapeutic potential of CHP NPs.

Taken together, these findings underscore the powerful dual action of CHP NPs in both suppressing pro-inflammatory pathways and enhancing anti-inflammatory responses. The HA-mediated targeted delivery and sustained release of CVL enable effective macrophage reprogramming, making CHP NPs a promising strategy for inflammation modulation and tissue regeneration. For example, IL-1ra acts as

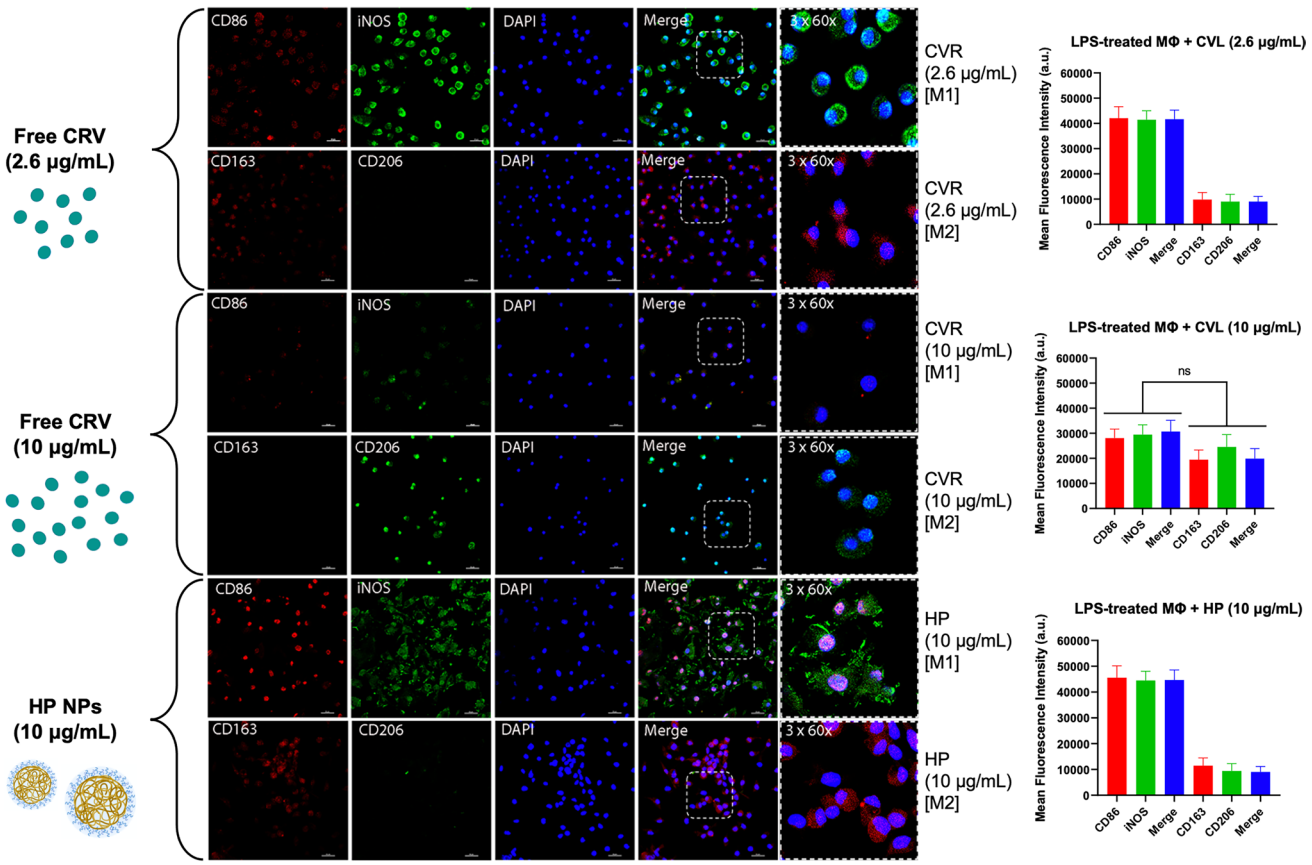

Fig. 5 LPS-treated macrophages were incubated with different concentrations of CVL (2.6 and 10 µg/mL) and HP NPs (10 µg/mL), to observe the difference in the marker expressions of M1-m and M2-m. Failure to see a significant increase in the M2-m marker expressions on incubation with HP NPs and free CVL, confirm the anti-inflammatory effect of CVL in CHP NPs. The total MFI calculated as described in Sect. 2.3.7. All values are expressed as mean ± SD ($n = 6$).

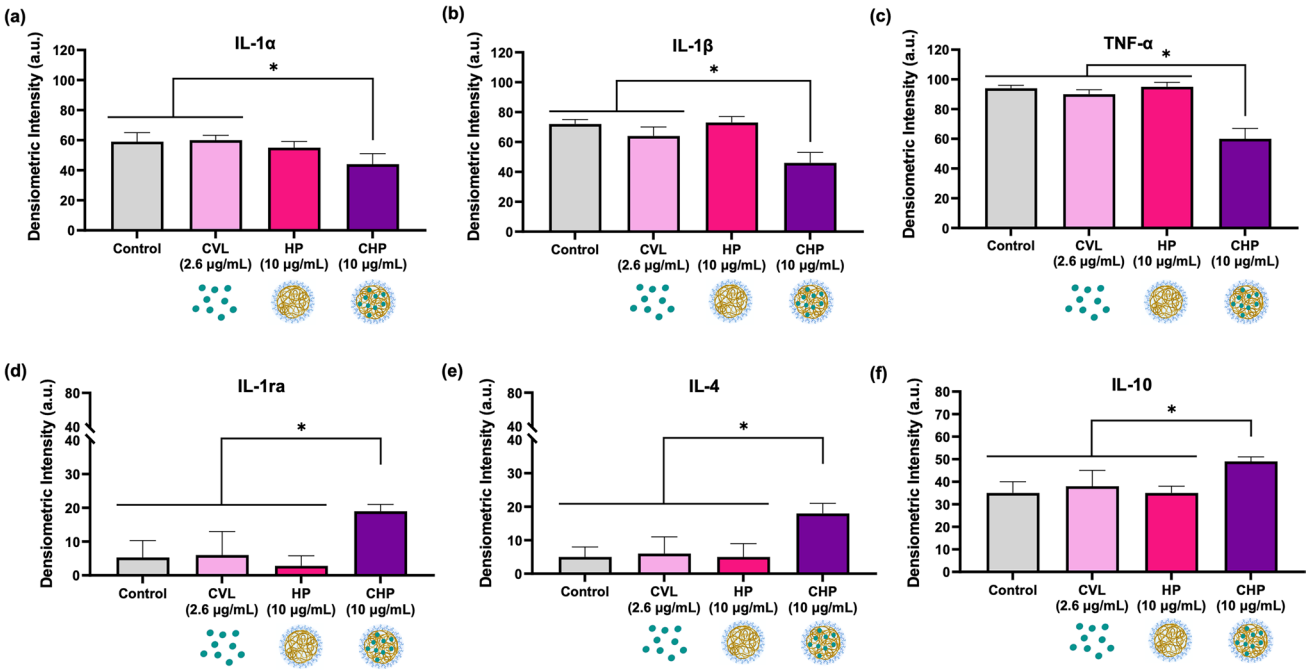

Fig. 6 The difference in the cytokine expressions in LPS-treated macrophages. (**a**) Decrease in pro-inflammatory cytokines, IL-1α/β and TNF-α, on treatment with CHP NPs and (**b**) increase in the anti-inflammatory cytokine expressions of IL-1ra/4/10. Immunoreactive spots were quantitated densitometrically using ImageJ software. The total MFI calculated as described in Sect. 2.3.7. All values are expressed as mean ± SD ($n = 3$), with $^*p < 0.05$.

a natural antagonist to IL-1α/β, competitively inhibiting their pro-inflammatory effects, while IL-4 and IL-10 are key regulators of M2 macrophage polarization and immune homeostasis. The dramatic upregulation of these cytokines indicates that CHP NPs not only suppresses inflammation but also actively promotes resolution and repair processes.

The dual action of CHP NPs, by downregulating pro-inflammatory and upregulating anti-inflammatory cytokines, points to a sophisticated mechanism of immune modulation. The HA coating facilitates targeted delivery to inflammatory macrophages, which are abundant in receptors for hyaluronic acid, ensuring that the nanoparticles reach their intended site of action. Once internalized, the slow and controlled release of CVL enables sustained suppression of inflammatory mediators while preventing macrophage activation from rebounding. Moreover, the enhanced expression of IL-4 and IL-10 suggests that CVL influences the signaling pathways that drive macrophage polarization from the pro-inflammatory M1 phenotype to the anti-inflammatory M2 phenotype, as demonstrated previously [12, 17–19]. To mention, also in this case, the control groups did not show any effect on the cytokine modulation levels.

These findings are particularly significant given the challenges associated with current anti-inflammatory therapies, which often lack specificity and have systemic side effects [94, 95]. By selectively targeting inflammatory macrophages and modulating their cytokine production, CHP NPs presents a novel therapeutic approach. The ability to simultaneously suppress harmful inflammation while enhancing reparative processes sets this system apart as an advanced and potentially transformative treatment for inflammatory diseases, including those involving chronic or excessive immune activation. Given the potent effects observed in cytokine modulation, CHP NPs has the potential to be adapted for a variety of clinical applications. Beyond the scope of this study, its use could be extended to conditions such as rheumatoid arthritis, inflammatory bowel disease, and even neuroinflammatory disorders. Furthermore, the platform versatility allows for modification with other bioactive agents, expanding its utility across a broad range of inflammatory and degenerative diseases.

Conclusion

In conclusion, this study demonstrates the successful development and characterization of hyaluronic acid (HA)-coated PLGA nanoparticles (CHP NPs) loaded with carvacrol (CVL), highlighting their potential in targeted anti-inflammatory therapy. The novelty lies in the integration of HA for macrophage-specific targeting via CD44-mediated uptake and the use of a single-emulsion solvent evaporation technique that yielded a remarkably high CVL encapsulation efficiency (~90%), surpassing previous methods. The

sustained release of CVL, along with enhanced M1-to-M2 macrophage repolarization and cytokine modulation, illustrates the therapeutic relevance of this platform. Importantly, the study not only confirms the physicochemical stability and functional efficacy of the nanoparticles but also provides mechanistic insights into how HA surface functionalization enhances cellular uptake and immune modulation. The demonstrated dose-dependent effects on inflammatory marker expression, along with controlled toxicity at therapeutic concentrations, underscore the translational promise of this nanosystem. Collectively, these findings pave the way for advancing CHP NPs as a clinically translatable nanotherapeutic for targeted inflammation control and immune modulation.

Supplementary Information The online version contains supplementary material available at https://doi.org/10.1007/s11095-025-04012-0.

Authors Contributions All authors contributed to the study conception and design. Material preparation, data collection and analysis were performed by Saniya Salathia and Dimitros Agas. The first draft of the manuscript was written by Saniya Salathia, Cristina Casadidio and Dimitros Agas and all authors commented on previous versions of the manuscript. All authors read and approved the final manuscript.

Funding This research was funded by European Commission H2020-MSCA-ITN-2020-PIANO, grant number 956477.

European Commission H2020-MSCA-ITN-2020-PIANO, 956477, Saniya Salathia

Data Availability The datasets generated during and/or analysed during the current study are available from the corresponding author on reasonable request.

Declarations

Ethics Approval and Consent to Participate All procedures involving animals were in compliance with the European Community Council Directive of 24 November 1986, and ethical approval was granted by the Italian ethical committee on Animal Experimentation (Authorization number: 1044/2024-PR).

Competing Interests The authors have no relevant financial or non-financial interests to disclose.

References

1. Farajzadeh R, Zarghami N, Serati-Nouri H, Momeni-Javid Z, Farajzadeh T, Jalilzadeh-Tabrizi S, et al. Macrophage repolarization using CD44-targeting hyaluronic acid–polylactide nanoparticles containing curcumin. Artif Cells Nanomed Biotechnol. 2017;46:1–9. https://doi.org/10.1080/21691401.2017.1408116.
2. Pan MH, Lai CS, Ho CT. Anti-inflammatory activity of natural dietary flavonoids. Food Funct. 2010;1:15–31. https://doi.org/10.1039/C0FO00103A.
3. Mitsi E, Kamng'ona R, Rylance J, Solórzano C, Jesus Reiné J, Mwandumba HC, et al. Human alveolar macrophages predominately express combined classical M1 and M2 surface markers in steady state. Respir Res. 2018;19:1–4. https://doi.org/10.1186/S12931-018-0777-0/FIGURES/1.
4. Rodríguez-Morales P, Franklin RA. Macrophage phenotypes and functions: resolving inflammation and restoring homeostasis. Trends Immunol. 2023;44:986–98. https://doi.org/10.1016/j.it.2023.10.004.
5. McWhorter FY, Wang T, Nguyen P, Chung T, Liu WF. Modulation of macrophage phenotype by cell shape. Proc Natl Acad Sci U S A. 2013;110:17253–8. https://doi.org/10.1073/PNAS.1308887110.
6. Chamorro Á, Hallenbeck J. The harms and benefits of inflammatory and immune responses in vascular disease. Stroke. 2006;37:291–3. https://doi.org/10.1161/01.STR.0000200561.69611.F8.
7. Jiang W, Zhang LX, Tan XY, Yu P, Dong M. Inflammation and histone modification in chronic pain. Front Immunol. 2023;13:1087648. https://doi.org/10.3389/FIMMU.2022.1087648/BIBTEX.
8. Campos EVR, Proença PLF, Oliveira JL, Pereira AES, De Morais Ribeiro LN, Fernandes FO, et al. Carvacrol and linalool co-loaded in β-cyclodextrin-grafted chitosan nanoparticles as sustainable biopesticide aiming pest control. Sci Rep. 2018;8:1–14. https://doi.org/10.1038/s41598-018-26043-x.
9. Duan WY, Zhu XM, Zhang SB, Lv YY, Zhai HC, Wei S, et al. Antifungal effects of carvacrol, the main volatile compound in *Origanum vulgare* L. essential oil, against *Aspergillus flavus* in postharvest wheat. Int J Food Microbiol. 2024. https://doi.org/10.1016/j.ijfoodmicro.2023.110514.
10. Iannitelli A, Grande R, di Stefano A, di Giulio M, Sozio P, Bessa LJ, et al. Potential antibacterial activity of carvacrol-loaded poly(DL-lactide-co-glycolide) (PLGA) nanoparticles against microbial biofilm. Int J Mol Sci. 2011;12:5039–51. https://doi.org/10.3390/IJMS12085039.
11. Ben Arfa A, Combes S, Preziosi-Belloy L, Gontard N, Chalier P. Antimicrobial activity of carvacrol related to its chemical structure. Lett Appl Microbiol. 2006;43:149–54. https://doi.org/10.1111/J.1472-765X.2006.01938.X.
12. Lima MDS, Quintans-Júnior LJ, De Santana WA, Martins Kaneto C, Pereira Soares MB, Villarreal CF. Anti-inflammatory effects of carvacrol: evidence for a key role of interleukin-10. Eur J Pharmacol. 2013;699:112–7. https://doi.org/10.1016/J.EJPHAR.2012.11.040.
13. Balaguer MP, Borne M, Chalier P, Gontard N, Morel MH, Peyron S, et al. Retention and release of cinnamaldehyde from wheat protein matrices. Biomacromol. 2013;14:1493–502. https://doi.org/10.1021/bm400158t.
14. Ates K, Yildiz ZI. Encapsulation of carvacrol in β-cyclodextrin metal-organic frameworks: improved solubility, stability, antioxidant capacity and controlled release of carvacrol. J Food Eng. 2025;391: 112445. https://doi.org/10.1016/J.JFOODENG.2024.112445.

15. Wang TH, Hsia SM, Wu CH, Ko SY, Chen MY, Shih YH, et al. Evaluation of the antibacterial potential of liquid and vapor phase phenolic essential oil compounds against oral microorganisms. PLoS ONE. 2016;11: e0163147. https://doi.org/10.1371/JOURNAL.PONE.0163147.
16. Simmons DL, Botting RM, Hla T. Cyclooxygenase isozymes: the biology of prostaglandin synthesis and inhibition. Pharmacol Rev. 2004;56:387–437. https://doi.org/10.1124/PR.56.3.3.
17. Hotta M, Nakata R, Katsukawa M, Hori K, Takahashi S, Inoue H. Carvacrol, a component of thyme oil, activates PPARα and γ and suppresses COX-2 expression. J Lipid Res. 2010;51:132–9. https://doi.org/10.1194/jlr.M900255-JLR200.
18. Yan C, Kuang W, Jin L, Wang R, Niu L, Xie C, et al. Carvacrol protects mice against LPS-induced sepsis and attenuates inflammatory response in macrophages by modulating the ERK1/2 pathway. Sci Rep. 2023;13(1): 12809. https://doi.org/10.1038/s41598-023-39665-7.
19. Mahmoodi M, Amiri H, Ayoobi F, Rahmani M, Taghipour Z, Ghavamabadi RT, et al. Carvacrol ameliorates experimental autoimmune encephalomyelitis through modulating pro- and anti-inflammatory cytokines. Life Sci. 2019;219:257–63. https://doi.org/10.1016/j.lfs.2018.11.051.
20. Wei HK, Xue HX, Zhou ZX, Peng J. A carvacrol-thymol blend decreased intestinal oxidative stress and influenced selected microbes without changing the messenger RNA levels of tight junction proteins in jejunal mucosa of weaning piglets. Animal. 2017;11:193–201. https://doi.org/10.1017/S1751731116001397.
21. Türkez H, Aydln E. Investigation of cytotoxic, genotoxic and oxidative properties of carvacrol in human blood cells. Toxicol Ind Health. 2016;32:625–33. https://doi.org/10.1177/0748233713506771.
22. Sampaio LA, Pina LTS, Serafini MR, Tavares DdosS, Guimarães AG. Antitumor effects of carvacrol and thymol: a systematic review. Front Pharmacol. 2021;12. https://doi.org/10.3389/fphar.2021.702487.
23. Llana-Ruiz-Cabello M, Gutiérrez-Praena D, Pichardo S, Moreno FJ, Bermúdez JM, Aucejo S, et al. Cytotoxicity and morphological effects induced by carvacrol and thymol on the human cell line Caco-2. Food Chem Toxicol. 2014;64:281–90. https://doi.org/10.1016/j.fct.2013.12.005.
24. Yammine J, Gharsallaoui A, Fadel A, Mechmechani S, Karam L, Ismail A, et al. Enhanced antimicrobial, antibiofilm and ecotoxic activities of nanoencapsulated carvacrol and thymol as compared to their free counterparts. Food Control. 2023. https://doi.org/10.1016/j.foodcont.2022.109317.
25. Xu J, Zhou F, Ji BP, Pei RS, Xu N. The antibacterial mechanism of carvacrol and thymol against *Escherichia coli*. Lett Appl Microbiol. 2008;47:174–9. https://doi.org/10.1111/J.1472-765X.2008.02407.X.
26. Liu YC, Zou XB, Chai YF, Yao YM. Macrophage polarization in inflammatory diseases. Int J Biol Sci. 2014;10:520. https://doi.org/10.7150/IJBS.8879.
27. de la Rios Rosa JM, Tirella A, Gennari A, Stratford IJ, Tirelli N. The CD44-mediated uptake of hyaluronic acid-based carriers in macrophages. Adv Healthc Mater. 2017;6. https://doi.org/10.1002/adhm.201601012.
28. Choi KY, Chung H, Min KH, Yoon HY, Kim K, Park JH, et al. Self-assembled hyaluronic acid nanoparticles for active tumor targeting. Biomaterials. 2010;31:106–14. https://doi.org/10.1016/J.BIOMATERIALS.2009.09.030.
29. Wickens JM, Alsaab HO, Kesharwani P, Bhise K, Amin MCIM, Tekade RK, et al. Recent advances in hyaluronic acid-decorated nanocarriers for targeted cancer therapy. Drug Discov Today. 2017;22:665–80. https://doi.org/10.1016/J.DRUDIS.2016.12.009.
30. Yadav AK, Mishra P, Mishra AK, Mishra P, Jain S, Agrawal GP. Development and characterization of hyaluronic acid–anchored PLGA nanoparticulate carriers of doxorubicin. Nanomedicine. 2007;3:246–57. https://doi.org/10.1016/J.NANO.2007.09.004.
31. Salathia S, Gigliobianco MR, Casadidio C, Di Martino P, Censi R. Hyaluronic acid-based nanosystems for CD44 mediated anti-inflammatory and antinociceptive activity. Int J Mol Sci. 2023;24(8): 7286. https://doi.org/10.3390/IJMS24087286.
32. Liu E, Zhou Y, Liu Z, Li J, Zhang D, Chen J, et al. Cisplatin loaded hyaluronic acid modified TiO2 nanoparticles for neoadjuvant chemotherapy of ovarian cancer. J Nanomater. 2015. https://doi.org/10.1155/2015/390358.
33. Pedrosa SS, Pereira P, Correia A, Gama FM. Targetability of hyaluronic acid nanogel to cancer cells: In vitro and in vivo studies. Eur J Pharm Sci. 2017. https://doi.org/10.1016/j.ejps.2017.03.045.
34. Isa ILM, Srivastava A, Tiernan D, Owens P, Rooney P, Dockery P, et al. Hyaluronic acid based hydrogels attenuate inflammatory receptors and neurotrophins in interleukin-1β induced inflammation model of nucleus pulposus cells. Biomacromol. 2015;16:1714–25. https://doi.org/10.1021/acs.biomac.5b00168.
35. Misra S, Hascall VC, Markwald RR, Ghatak S. Interactions between hyaluronan and its receptors (CD44, RHAMM) regulate the activities of inflammation and cancer. Front Immunol 2015;6. https://doi.org/10.3389/fimmu.2015.00201.
36. Manca ML, Castangia I, Zaru M, Nácher A, Valenti D, Fernàndez-Busquets X, et al. Development of curcumin loaded sodium hyaluronate immobilized vesicles (hyalurosomes) and their potential on skin inflammation and wound restoring. Biomaterials. 2015;71:100–9. https://doi.org/10.1016/j.biomaterials.2015.08.034.
37. Kita K, Dittrich C. Drug delivery vehicles with improved encapsulation efficiency: taking advantage of specific drug-carrier interactions. Expert Opin Drug Deliv. 2011;8:329–42. https://doi.org/10.1517/17425247.2011.553216.
38. Kim MR, Feng T, Zhang Q, Chan HYE, Chau Y. Co-encapsulation and co-delivery of peptide drugs via polymeric nanoparticles. Polymers (Basel). 2019. https://doi.org/10.3390/POLYM11020288.
39. Klojdová I, Milota T, Smetanová J, Stathopoulos C. Encapsulation: a strategy to deliver therapeutics and bioactive compounds? Pharmaceuticals. 2023. https://doi.org/10.3390/PH16030362.
40. Michiels J, Missotten J, Dierick N, Fremaut D, Maene P, De Smet S. In vitro degradation and in vivo passage kinetics of carvacrol, thymol, eugenol and trans-cinnamaldehyde along the gastrointestinal tract of piglets. J Sci Food Agric. 2008;88:2371–81. https://doi.org/10.1002/JSFA.3358.
41. Andersen A. Final report on the safety assessment of sodium p-Chloro-m-Cresol, p-chloro-m-cresol, chlorothymol, mixed cresols, m-cresol, o-cresol, p-cresol, isopropyl cresols, thymol, o-cymen-5-ol, and carvacrol. Int J Toxicol. 2006;25:29–127. https://doi.org/10.1080/10915810600716653.
42. Feketa VV, Marrelli SP. Systemic administration of the TRPV3 ion channel agonist carvacrol induces hypothermia in conscious rodents. PLoS ONE. 2015;10: e0141994. https://doi.org/10.1371/JOURNAL.PONE.0141994.
43. Mączka W, Twardawska M, Grabarczyk M, Wińska K. Carvacrol—a natural phenolic compound with antimicrobial properties. Antibiotics. 2023;12: 824. https://doi.org/10.3390/ANTIBIOTICS12050824.
44. Pradhan R, Ramasamy T, Choi JY, Kim JH, Poudel BK, Tak JW, et al. Hyaluronic acid-decorated poly(lactic-co-glycolic acid) nanoparticles for combined delivery of docetaxel and tanespimycin. Carbohydr Polym. 2015;123:313–23. https://doi.org/10.1016/J.CARBPOL.2015.01.064.
45. Fay F, Quinn DJ, Gilmore BF, McCarron PA, Scott CJ. Gene delivery using dimethyldidodecylammonium bromide-coated

PLGA nanoparticles. Biomaterials. 2010;31:4214–22. https://doi.org/10.1016/j.biomaterials.2010.01.143.
46. Abdelmonem A, Zhang Y, Braunschweig B, Glikman D, Rumpel A, Peukert W, et al. Adsorption of CTAB on sapphire- c at high pH: surface and zeta potential measurements combined with sum-frequency and second-harmonic generation. Langmuir. 2022;38:3380–91. https://doi.org/10.1021/acs.langmuir.1c03069.
47. Cosco D, Mare R, Paolino D, Salvatati MC, Cilurzo F, Fresta M. Sclareol-loaded hyaluronan-coated PLGA nanoparticles: physico-chemical properties and in vitro anticancer features. Int J Biol Macromol. 2019;132:550–7. https://doi.org/10.1016/J.IJBIOMAC.2019.03.241.
48. Sheybanifard M, Beztsinna N, Bagheri M, Buhl EM, Bresseleers J, Varela-Moreira A, et al. Systematic evaluation of design features enables efficient selection of Π electron-stabilized polymeric micelles. Int J Pharm. 2020;584: 119409. https://doi.org/10.1016/J.IJPHARM.2020.119409.
49. Gil D, Frank-Kamenetskii A, Barry J, Reukov V, Xiang Y, Das A, et al. Albumin-assisted method allows assessment of release of hydrophobic drugs from nanocarriers. Biotechnol J. 2018;13:1700337. https://doi.org/10.1002/BIOT.201700337;SUBPAGE:STRING:FULL.
50. Paál K, Müller J, Hegedûs L. High affinity binding of paclitaxel to human serum albumin. Eur J Biochem. 2001;268:2187–91. https://doi.org/10.1046/J.1432-1327.2001.02107.X.
51. Wang Y, Fens MH, van Kronenburg NCH, Shi Y, Lammers T, Heger M, et al. Magnetic beads for the evaluation of drug release from biotinylated polymeric micelles in biological media. J Control Release. 2022;349:954–62. https://doi.org/10.1016/J.JCONREL.2022.07.044.
52. Dash S, Murthy PN, Nath L, Chowdhury P. Kinetic modeling on drug release from controlled drug delivery systems. Acta Pol Pharm Drug Res. 2010;67:217–23.
53. Stulzer HK, Tagliari MP, Parize AL, Silva MAS, Laranjeira MCM. Evaluation of cross-linked chitosan microparticles containing acyclovir obtained by spray-drying. Mater Sci Eng C Mater Biol Appl. 2009;29:387–92. https://doi.org/10.1016/j.msec.2008.07.030.
54. Agas D, Marchegiani A, Laus F, Gabai V, Sufianov AA, Shneider A, et al. p62/SQSTM1 indirectly mediates remote multipotent mesenchymal cells and rescues bone loss and bone marrow integrity in ovariectomized rats. J Cell Physiol. 2023;238:407–19. https://doi.org/10.1002/jcp.30937.
55. Brugger W, Kreutz M, Andreesen R. Macrophage colony-stimulating factor is required for human monocyte survival and acts as a cofactor for their terminal differentiation to macrophages in vitro. J Leukoc Biol. 1991;49:483–8. https://doi.org/10.1002/jlb.49.5.483.
56. Kim M, An J, Shin SA, Moon SY, Kim M, Choi S, et al. Anti-inflammatory effects of TP1 in LPS-induced Raw264.7 macrophages. Appl Biol Chem. 2024. https://doi.org/10.1186/s13765-024-00873-y.
57. Guo H, Jing L, Xia C, Zhu Y, Xie Y, Ma X, et al. Copper promotes LPS-induced inflammation via the NF-κB pathway in bovine macrophages. Biol Trace Elem Res. 2024. https://doi.org/10.1007/s12011-024-04107-6.
58. Agas D, Sabbieti MG, Marchetti L, Xiao L, Hurley MM. FGF-2 enhances Runx-2/Smads nuclear localization in BMP-2 canonical signaling in osteoblasts. J Cell Physiol. 2013;228:2149–58. https://doi.org/10.1002/jcp.24382.
59. Barros MHM, Hauck F, Dreyer JH, Kempkes B, Niedobitek G. Macrophage polarisation: an immunohistochemical approach for identifying M1 and M2 macrophages. PLoS ONE. 2013. https://doi.org/10.1371/journal.pone.0080908.
60. Spadea A, Rios De La Rosa JM, Tirella A, Ashford MB, Williams KJ, Stratford IJ, et al. Evaluating the efficiency of hyaluronic acid for tumor targeting via CD44. Mol Pharm. 2019;16:2481–93. https://doi.org/10.1021/acs.molpharmaceut.9b00083.
61. Mukerjee A, Vishwanatha JK. Formulation, characterization and evaluation of curcumin-loaded PLGA nanospheres for cancer therapy. Anticancer Res. 2009;29:3867.
62. Casadidio C, Mayol L, Biondi M, Scuri S, Cortese M, Hennink WE, et al. Anionic polysaccharides for stabilization and sustained release of antimicrobial peptides. Int J Pharm. 2023. https://doi.org/10.1016/j.ijpharm.2023.122798.
63. Dovedytis M, Liu ZJ, Bartlett S. Hyaluronic acid and its biomedical applications: a review. Engineered Regeneration. 2020;1:102–13. https://doi.org/10.1016/J.ENGREG.2020.10.001.
64. Tampau A, González-Martinez C, Chiralt A. Carvacrol encapsulation in starch or PCL based matrices by electrospinning. J Food Eng. 2017;214:245–56. https://doi.org/10.1016/J.JFOODENG.2017.07.005.
65. Gursul S, Karabulut I, Durmaz G. Antioxidant efficacy of thymol and carvacrol in microencapsulated walnut oil triacylglycerols. Food Chem. 2019;278:805–10. https://doi.org/10.1016/J.FOODCHEM.2018.11.134.
66. Singh R, Kesharwani P, Mehra NK, Singh S, Banerjee S, Jain NK. Development and characterization of folate anchored Saquinavir entrapped PLGA nanoparticles for anti-tumor activity. Drug Dev Ind Pharm. 2015;41:1888–901. https://doi.org/10.3109/03639045.2015.1019355.
67. Pan NC, Pereira HCB, da Silva MLC, Vasconcelos AFD, Celligoi MAPC. Improvement production of Hyaluronic acid by *Streptococcus zooepidemicus* in sugarcane molasses. Appl Biochem Biotechnol. 2017;182:276–93. https://doi.org/10.1007/s12010-016-2326-y.
68. Prát T, Vladimír Velebný KN. Hyaluronic acid as effective cryoprotective agent for hMSC cryopreservation. Cryobiology. 2022;109:47. https://doi.org/10.1016/J.CRYOBIOL.2022.11.150.
69. Fonte P, Soares S, Costa A, Andrade JC, Seabra V, Reis S, et al. Effect of cryoprotectants on the porosity and stability of insulin-loaded PLGA nanoparticles after freeze-drying. Biomatter. 2012;2:329. https://doi.org/10.4161/BIOM.23246.
70. Andreana I, Bincoletto V, Manzoli M, Rodà F, Giarraputo V, Milla P, et al. Freeze Drying of Polymer Nanoparticles and Liposomes Exploiting Different Saccharide-Based Approaches. Materials. 2023;16:1212. https://doi.org/10.3390/MA16031212/S1.
71. Sun H, Jiao R, An G, Xu H, Wang D. Influence of particle size on the aggregation behavior of nanoparticles: role of structural hydration layer. J Environ Sci (China). 2021;103:33–42. https://doi.org/10.1016/j.jes.2020.10.007.
72. Lim YW, Tan WS, Ho KL, Mariatulqabtiah AR, Kasim NHA, Abd Rahman N, et al. Challenges and Complications of Poly(lactic-co-glycolic acid)-Based Long-Acting Drug Product Development. Pharmaceutics 2022;14. https://doi.org/10.3390/PHARMACEUTICS14030614.
73. Xu Y, Kim CS, Saylor DM, Koo D. Polymer degradation and drug delivery in PLGA-based drug–polymer applications: a review of experiments and theories. J Biomed Mater Res B Appl Biomater. 2017;105:1692–716. https://doi.org/10.1002/JBM.B.33648.
74. Li J, Pu Y, Wang S, Ding M, Chen D, Zhu M. Pharmacokinetic study and effectiveness evaluation of slow-release PLGA-5-fluorouracil microsphere. Cancer Chemother Pharmacol. 2013;71:351–9. https://doi.org/10.1007/S00280-012-2016-6/METRICS.
75. Fredenberg S, Wahlgren M, Reslow M, Axelsson A. The mechanisms of drug release in poly(lactic-co-glycolic acid)-based drug delivery systems—a review. Int J Pharm. 2011;415:34–52. https://doi.org/10.1016/J.IJPHARM.2011.05.049.
76. Son GH, Lee BJ, Cho CW. Mechanisms of drug release from advanced drug formulations such as polymeric-based drug-delivery systems and lipid nanoparticles. J Pharm Investig. 2017;47:287–96. https://doi.org/10.1007/s40005-017-0320-1.

77. Chen Y, Wang S, Wang S, Liu C, Su C, Hageman M, et al. Initial drug dissolution from amorphous solid dispersions controlled by polymer dissolution and drug-polymer interaction. Pharm Res. 2016;33:2445–58. https://doi.org/10.1007/s11095-016-1969-2.
78. Keawchaoon L, Yoksan R. Preparation, characterization and in vitro release study of carvacrol-loaded chitosan nanoparticles. Colloids Surf B Biointerfaces. 2011;84:163–71. https://doi.org/10.1016/j.colsurfb.2010.12.031.
79. Niza E, Božik M, Bravo I, Clemente-Casares P, Lara-Sanchez A, Juan A, et al. PEI-coated PLA nanoparticles to enhance the antimicrobial activity of carvacrol. Food Chem. 2020. https://doi.org/10.1016/j.foodchem.2020.127131.
80. Krepker M, Prinz-Setter O, Shemesh R, Vaxman A, Alperstein D, Segal E. Antimicrobial carvacrol-containing polypropylene films: composition, structure and function. Polymers (Basel). 2018;10. https://doi.org/10.3390/polym10010079.
81. Taghipour B, Yakhchali M, Haririan I, Tamaddon AM, Samani SM. The effects of technical and compositional variables on the size and release profile of bovine serum albumin from PLGA based particulate systems. Res Pharm Sci. 2014;9:407–20.
82. Bračič M, Fras-Zemljič L, Pérez L, Kogej K, Stana-Kleinschek K, Kargl R, et al. Protein-repellent and antimicrobial nanoparticle coatings from hyaluronic acid and a lysine-derived biocompatible surfactant. J Mater Chem B. 2017. https://doi.org/10.1039/C7TB00311K.
83. Almalik A, Benabdelkamel H, Masood A, Alanazi IO, Alradwan I, Majrashi MA, et al. Hyaluronic acid coated chitosan nanoparticles reduced the immunogenicity of the formed protein corona. Sci Rep. 2017. https://doi.org/10.1038/S41598-017-10836-7.
84. Torchilin VP. Drug targeting. Eur J Pharm Sci. 2000. https://doi.org/10.1016/S0928-0987(00)00166-4.
85. Vasir J, Reddy M, Labhasetwar V. Nanosystems in drug targeting: opportunities and challenges. Curr Nanosci. 2006;1:47–64. https://doi.org/10.2174/157341306052953110.
86. Cunha C, Gomes C, Vaz AR, Brites D. Exploring new inflammatory biomarkers and pathways during LPS-induced M1 polarization. Mediators Inflamm. 2016. https://doi.org/10.1155/2016/6986175.
87. Binnemars-Postma KA, Ten Hoopen HW, Storm G, Prakash J. Differential uptake of nanoparticles by human M1 and M2 polarized macrophages: protein corona as a critical determinant. Nanomedicine. 2016;11:2889–902. https://doi.org/10.2217/nnm-2016-0233.
88. Li Q, Li C, Tong W. *Nile* red loaded PLGA nanoparticles surface modified with Gd-DTPA for potential dual-modal imaging. J Nanosci Nanotechnol. 2016;16:5569–76. https://doi.org/10.1166/jnn.2016.11735.
89. Zhang Y, Chen Q, Nai Y, Cao C. Suppression of miR-155 attenuates neuropathic pain by inducing an M1 to M2 switch in microglia. Folia Neuropathol. 2020;58:70–82. https://doi.org/10.5114/FN.2020.94008.
90. Tian X, Liu H, Xiang F, Xu L, Dong Z. β-Caryophyllene protects against ischemic stroke by promoting polarization of microglia toward M2 phenotype via the TLR4 pathway. Life Sci. 2019;237:116915. https://doi.org/10.1016/J.LFS.2019.116915.
91. Lisi L, Ciotti GMP, Braun D, Kalinin S, Currò D, Dello Russo C, et al. Expression of iNOS, CD163 and ARG-1 taken as M1 and M2 markers of microglial polarization in human glioblastoma and the surrounding normal parenchyma. Neurosci Lett. 2017;645:106–12. https://doi.org/10.1016/J.NEULET.2017.02.076.
92. Kosovrasti VY, Nechev LV, Amiji MM. Peritoneal macrophage-specific TNF-α gene silencing in LPS-induced acute inflammation model using CD44 targeting hyaluronic acid nanoparticles. Mol Pharm. 2016;13:3404–16. https://doi.org/10.1021/ACS.MOLPHARMACEUT.6B00398/SUPPL_FILE/MP6B00398_SI_001.PDF.
93. Schleicher U, Paduch K, Debus A, Obermeyer S, König T, Kling JC, et al. TNF-mediated restriction of arginase 1 expression in myeloid cells triggers type 2 NO synthase activity at the site of infection. Cell Rep. 2016;15:1062–75. https://doi.org/10.1016/J.CELREP.2016.04.001.
94. Rainsford KD. Profile and mechanisms of gastrointestinal and other side effects of nonsteroidal anti-inflammatory drugs (NSAIDs). Am J Med. 1999;107:27–35. https://doi.org/10.1016/S0002-9343(99)00365-4.
95. Pountos I, Georgouli T, Bird H, Giannoudis PV. Nonsteroidal anti-inflammatory drugs: prostaglandins, indications, and side effects. Int J Interferon Cytokine Mediat Res. 2011;3:19–27. https://doi.org/10.2147/IJICMR.S10200.